Università Politecnica delle Marche

FACOLTÀ DI INGEGNERIA
Corso di Laurea Triennale in Ingegneria Civile e Ambientale

Effect of the soil spatial variability on the ultimate bearing capacity of foundations

Effetto della variabilita spaziale del suolo sulla capacita portante ultima delle fondazione

Tesi di laurea di: Maya Al Boustany

Relatore: Chiar.mo

Prof. *DAVI' FABRIZIO*

Anno Accademico: 2019 - 2020

ABSTRACT

The aim of this project is to study the performance of shallow foundations resting on spatially varying soils using probabilistic approaches and perform a simple building structural design.

In the first part of this project, a static loading was considered in the probabilistic analysis. In this part, only the soil spatial variability was considered and the soil parameters were modelled by random fields. In such cases, Monte Carlo Simulation (MCS) methodology is generally used in literature. In this project, the Sparse Polynomial Chaos Expansion (SPCE) methodology was employed. This methodology aims at replacing the finite element/finite difference deterministic model by a meta-model. This leads (in the present case of highly dimensional stochastic problems) to a significant reduction in the number of calls of the deterministic model with respect to the crude MCS methodology. Moreover, an efficient combined use of the SPCE methodology and the Global Sensitivity Analysis (GSA) was proposed. The aim is to reduce once again the probabilistic computation time for problems with expensive deterministic models.

In the second part, a simple building structural design was made, in order to practice on the use of softwares and make the reinforcement of the main structural elements of the building.

Contents

CHAPTER I. LITERATURE REVIEW.....16
I.1 Introduction……16
I.2 Sources of uncertainties…….…17
I.3 Modeling of uncertain parameters…….…17
I.3.1 Modeling parameters by random variables……....18
I.3.2 Modeling uncertainties of soil by a random field…….…18
I.3.3 The expansion optimal linear estimation (EOLE) method for random field discretization…….…21
I.3.4 The simulation methods……23
I.4 The metamodeling techniques……24
I.4.1 The Polynomial chaos expansion PCE methodology - the classical truncation scheme…….24
I.4.2 Sparse Polynomial Chaos Expansion (SPCE) methodology..28
I.4.3 SPCE/GSA……..30
I.5 FLAC^{3D}……..32
CHAPTER II. EFFECT OF THE SOIL SPATIAL VARIABILITY IN THREE DIMENSIONS ON THE ULTIMATE BEARING CAPACITY OF SQUARE FOUNDATIONS……...33
II.1 Introduction……..……..33
II.2 Probabilistic analysis of square footing resting on a 3d spatially varying soil mass…….33
II.3 Numerical results……35
II.3.1 Deterministic numerical results…….35
II.3.2 Probabilistic numerical results……..36
CHAPTER III. EFFECT OF THE SOIL SPATIAL VARIABILITY IN THREE DIMENSIONS ON THE ULTIMATE BEARING CAPACITY OF RECTANGULAR FOUNDATIONS.....43
III.1 Introduction……43
III.2 Probabilistic analysis of square footing resting on a 3d spatially varying soil mass…….43
III.3 Numerical results……45
III.3.1 Deterministic numerical results…….45
III.3.2 Probabilistic numerical results……...45
III.3.3 Discussion……..51
III.4 Conclusions……52
CHAPTER IV. BUILDING DESIGN.....54
IV.1 Introduction……54
IV.2 Description of the project……...54

IV.2.1 Plans description……55
IV.2.2 Lateral elevation……58
IV.3 Structural design and design criteria……...58
IV.3.1 Loadings……58
IV.3.2 Design criteria……60
IV.4 Model on Etabs……...61
IV.4.1 Etabs data input……61
IV.4.2 Story data……..64
IV.4.3 Etabs output views……65
IV.4.4 Structure verification……67
IV.4.5 Conclusion……72
IV.5 Column design……...72
IV.5.1 Introduction……..72
IV.5.2 Types of columns……73
IV.5.3 ACI code provisions for column design……..73
IV.5.4 Hints for design according to the ACI building requirement code……...74
IV.5.5 Design of columns……75
IV.6 Shear wall design……..76
IV.6.1 Introduction……79
IV.6.2 Analysis criteria in Etabs……79
IV.6.3 Design of the shear wall……...80
IV.7 Slab design……81
IV.7.1 Introduction……..81
IV.7.2 Preliminary sizing of the slab……...81
IV.7.3 Design on SAFE……...82
IV.7.4 Maximum allowable Deflection……...83
IV.7.5 Loads……80
IV.7.6 Results on SAFE……..84
IV.8 Raft foundation design……90
IV.8.1 Design of mat foundation……90
IV.8.2 Modeling process.....90
IV.8.3 Safe model……...91
IV.8.4 Moments……..94
IV.8.5 Reinforcement of the raft……94
IV.8.6 Reinforcement details……..96
General conclusion……94
References……..95
Appendix A……96

List of figures

Figure II.1. Mesh used for the computation of the ultimate bearing capacity of a square footing 36

Figure II.2. Perspective view of half of the soil domain showing (a) a random field realization (the contour lines provide the distribution of the soil cohesion on the envelope of this domain) and (b) the contours of the strain rate 40

Figure II.3. Influence of the mean value of the cohesion on the PDF of the bearing capacity coefficient N_c of a strip footing when using 3D random field for a_h=10m, a_v=1m and COV_c=25% 41

Figure III.1. Mesh used for the computation of the ultimate bearing capacity of a rectangular footing 45

Figure III.2. Perspective view of the soil domain showing (a) a random field realization (the contour lines provide the distribution of the soil cohesion on the envelope of this domain) and (b) the contours of the strain rate 48

Figure III.3. PDF of the bearing capacity coefficient N_c of a rectangular footing when using 3D random field for a_h=9m, a_v=1m and COV_c=25%.. 49

Figure IV.1. Building front elevation 55

Figure IV.2. Ground floor plan 56

Figure IV.3. Mezzanine story plan 57

Figure IV.4. Repetitive story plan..... 58

Figure IV.5. Vertical cut section of the building 59

Figure IV.6. DXF floor plan of repetitive story 63

Figure IV.7. 3D view on Etabs 66

Figure IV.8. Plan view on Etabs 67

Figure IV.9. Deformed shape due to dead loads……..67

Figure IV.10. Deformed shape due to (a) EQX and (b) SpecX……68

Figure IV.11. Maximum story displacement due to WindX 69

Figure IV.12. Maximum story displacement dur to WindY 70
Figure IV.13. Maximum story displacement due to SpecX..... 70
Figure IV.14. Maximum story displacement due to Specy 71
Figure IV.15. Maximum story drift due to WindX..... 71
Figure IV.16. Maximum story drift due to WindY..... 72
Figure IV.17. Maximum story drift due to SpecX..... 72
Figure IV.18. Maximum story drift due to SpecY..... 73
Figure IV.19. Chosen column for design..... 77
Figure IV.20. Steel reinforcement of column C13 provided by S-concrete at story 1 78
Figure IV.21. Longitudinal cut section of column C13 79
Figure IV.22. Chosen shear wall for design 81
Figure IV.23. Reinforcement of shear wall provided by S-concrete at story 1 .. 82
Figure IV.24. Floor plan mesh on SAFE 84
Figure IV.25. Deformed shape under service loads..... 85
Figure IV.26. 3D view of the deformed shape..... 86
Figure IV.27. Mxx (KN.m/m) under ultimate combination 86
Figure IV.28. Myy (KN.m/m) under ultimate combination 87
Figure IV.29. Top rebar Intensity-Direction 1..... 87
Figure IV.30. Top rebar Intensity-Direction 2..... 88
Figure IV.31. Bottom rebar Intensity-Direction 89
Figure IV.32. Bottom rebar Intensity-Direction 2 89
Figure IV.33. Top reinforcement..... 90
Figure IV.34. Bottom reinforcement 90
Figure IV.35. Deformed shape under service loads..... 92
Figure IV.36. Soil pressure under the raft foundation due to service load 93
Figure IV.37. Punching shear ratios with 1.2m thickness 94
Figure IV.38. Punching shear ratios with 1.35m thickness 95
Figure IV.39. Mxx (KN.m/m) under ultimate combination 95

Figure IV.40. Myy (KN.m/m) under ultimate combination 95
Figure IV.41. Top rebar intensity-direction 1 & 2..... 96
Figure IV.42. Bottom rebar intensity-direction 1 & 2 96
Figure IV.43. Reinforcement detail for raft foundation..... 96

List of tables

Table I.1. Theoretical ACF used to determine the autocorrelation distance (a) [Vanmarcke (1983)] 21

Table II.1. Number of random variables needed to discretize the 3D cohesion random fields in the case of the square footing..... 39

Table II.2. Effect of the isotropic autocorrelation distance (a) on the statistical moments μ_{N_c} and σ_{N_c} of the bearing capacity coefficient N_c of square footing using 3D random field..... 42

Table II.3. Effect of the vertical autocorrelation distance (a_v) on the statistical moments μ_{N_c} and σ_{N_c} of the bearing capacity coefficient N_c of square footing using 3D random field..... 42

Table II.4. Effect of the horizontal autocorrelation distance (a_h) on the statistical moments μ_{N_c} and σ_{N_c} of the bearing capacity coefficient N_c of square footing using 3D random field..... 43

Table III.1. Number of random variables needed to discretize the 3D cohesion random fields in the case of the rectangular footing. 47

Table III.2. Effect of the isotropic autocorrelation distance (a) on the statistical moments μ_{N_c} and σ_{N_c} of the bearing capacity coefficient N_c of rectangular footing using 3D random field 50

Table III.3. Effect of the vertical autocorrelation distance (a_v) on the statistical moments μ_{N_c} and σ_{N_c} of the bearing capacity coefficient N_c of rectangular footing using 3D random field 51

Table III.4. Effect of the horizontal autocorrelation distance (a_h) on the statistical moments μ_{N_c} and σ_{N_c} of the bearing capacity coefficient N_c of rectangular footing using 3D random field 51

Table III.5. Ratios between the coefficients of variation values of N_c (obtained using 3D random field) for the square footing..... 52

Table IV.1. Earthquake input data 61
Table IV.2. Static load cases 64
Table IV.3. Load combinations 65
Table IV.4. Story data 66
Table IV.5. Periods and modal participation mass ratio 69

Abbreviations

SPT: Standard Penetration Test

ACF: Autocorrelation Function

VST: Vane Shear Test

Q_u: Unconfined compressive strength test

UU: Unconfined Undrained triaxial test

DSS: Direct Shear Test

CPT: Cone Penetration Test

DMT: Dilatometer Test

C_u: undrained shear strength

EOLE: The Expansion Optimal Linear Estimation method

MCS: Universal Monte Carlo Simulation methodology

PDF: Probability Density Function

PCE: Polynomial Chaos Expansion methodology

SPCE: Sparse Polynomial Chaos Expansion methodology

GSA: Global Sensitivity Analysis

ED: Experimental Design

Symbols

$Z(x)$: random variable

a: autocorrelation distance

δ: scale of fluctuation

ρ: correlation coefficient

X: location vector

COV: covariance

E[.]: expected value

μ_Z: mean of the property Z

σ_Z: standard deviation of the property Z

Δh: separation distance

K: vector of values Z

s: number of data samples

K: maximum allowable number of lags

$\Sigma_{\chi;\chi}$: autocorrelation matrix

ξ_j : independent standard normal random variables

λ_j, ϕ_j : eigenvalues & eigenvectors of $\Sigma_{\chi;\chi}$

ε: tolerance

α_β: unknown PCE coefficients

Ψ_β: multivariate Hermite polynomials

R^2: coefficient of determination

c: cohesion

q_{ult}: ultimate bearing capacity

General introduction

Traditionally, the analysis and design of geotechnical structures are based on deterministic approaches. In these approaches, constant conservative values of the soil and/or the loading parameters are considered with no attempt to characterize and model the uncertainties related to these parameters. In such approaches, a global safety factor is applied to take into account the soil and loading uncertainties. The choice of this factor is based on the judgment of the engineer based on his past experience.

During the last recent years, much effort has been paid for the establishment of more reliable and efficient methods based on probabilistic analysis. It should be mentioned here that in any probabilistic analysis, there are two tasks that must be performed. First, it is necessary to identify and quantify the soil uncertainties. This task is usually carried out through experimental investigations and expert judgment. Although this first step is extremely important, it will not be considered throughout this work. The values of the soil and loading uncertainties used in the analysis are taken from the literature. After the input uncertainties have been appropriately quantified, the task remains to quantify the influence of these uncertainties on the output of the model. This task is referred to as uncertainty propagation. In other words, the uncertainty propagation aims to study the impact of the input uncertainty on the variation of a model output (response).

The ultimate aim of this work is to study the performance of shallow foundations resting on spatially varying soils using probabilistic approaches.

In the first part of this thesis (i.e. chapters II and III), static loading cases were considered in the probabilistic analysis. In this part, only the soil spatial variability was considered and the soil parameters were modelled by random fields. The system responses were the ultimate bearing capacity of the foundation.

Before the presentation of the different probabilistic analyses performed in this project, a literature review is presented in chapter I. It presents (i) the different sources of uncertainties, (ii) the soil spatial variability, (iii) the different meta-modeling techniques for uncertainty propagation and finally, (iv) the PCE and the SPCE methodologies which are the methods used in this thesis.

Contrary to the existing literature where the very computationally-expensive Monte Carlo Simulation (MCS) methodology is generally used to determine the probability density function (PDF) of a high-dimensional stochastic system involving spatially varying soil/rock properties; in chapters II and III, the Sparse Polynomial Chaos Expansion (SPCE) and its extension 'the combined use of the SPCE and the Global Sensitivity Analysis (GSA)' are employed in the framework of the probabilistic analysis. Notice that the sparse polynomial chaos expansion is an extension of the Polynomial Chaos Expansion (PCE). A PCE or a SPCE methodology aims at replacing the finite element/finite difference deterministic model by a meta-model (i.e. a simple analytical equation). Thus, within the framework of the PCE or the SPCE methodology, the PDF of the system response can be easily obtained. This is because MCS is no longer applied on the original computationally-expensive deterministic model, but on the meta-model. The deterministic models used to calculate the system responses are based on numerical simulations using the commercial software FLAC^{3D}.

In chapters chapter II & III, the SPCE methodology was used to investigate the effect of the spatial variability in three dimensions (3D) through the study of the ultimate bearing capacity of square & rectangular foundations resting on a purely cohesive soil with a spatially varying cohesion in the three dimensions.

In the second part of this project (chapter IV), a study of a simple residential building was done. The design was made using many softwares (e.g. Etabs, SAFE, etc…). The structural design was performed to the main structural elements of the building. Reinforcement details were presented in this chapter.

CHAPTER I. LITERATURE REVIEW

I.1 Introduction

Geotechnical analyzes are generally based on deterministic approaches that consider conservative values of design parameters. These approaches determine a safety factor, which takes into account the uncertainty of the ground and the load. Deterministic models typically use a single discrete descriptor for the parameter of interest.

“Certainty” refers to situations in which the outcome of an event or the value of a parameter is known with unit probability.

Uncertainty analysis is an emerging approach that uses estimation and simulation techniques to consider the variability of available data and to estimate the frequency with which values of interest are likely to be exceeded. While it has not yet been widely applied in geotechnical engineering practice, this approach offers insight into existing data for heterogeneous geotechnical systems.

Uncertainty pervades many aspects of geotechnical engineering, particularly in the characterization of soil properties. In general, some of this uncertainty may be due to the difficulty in making accurate measurements and some may be due to uncertainty in the models, equations, and understanding of the systems involved. Additional uncertainty can result from the spatial variability of the system.

Uncertainty in geotechnical soil properties can be formally grouped into aleatory and epistemic uncertainty (Lacasse et al., 1996). Aleatory uncertainty represents the natural randomness of a property and, as such, is a function of the spatial variability of the property. Recognizing spatial variability is important because it can help distinguish the distances over which it occurs compared to the scale of the data of interest (Whitman, 1996). Epistemic uncertainty results from a lack of information and shortcomings in measurement and/or calculation. Epistemic uncertainty includes the systematic error resulting from factors such as the method of property measurement, the quantity of available data, and modeling errors.

Human error would be considered a third source of uncertainty, however it is not considered in this overview because it is difficult to isolate and its effect on probability is usually included in compilations of statistics on aleatory uncertainty.

I.2 Sources of uncertainties

While many sources of uncertainties may exist, they are generally categorized as either aleatory or epistemic [Der Kiureghian and Ditlevsen (2009)].

Sources of epistemic uncertainty could include non-standard equipment (such as the sampler size, deformed samplers or rods, rod length, hammer drop system, hammer weight, etc., not conforming to the SPT standard), and insufficient data to form reasonable statistics, such as one boring over a large site. It is important to note that epistemic uncertainty can usually be reduced by acquisition of additional data or improvements in measurement procedures.

I.3 Modeling of uncertain parameters

All probabilistic approaches, simplified or advanced, consider the uncertainties of soil parameters. The simplified approach, considering the uncertain parameters as aleatory variables defined by a stochastic distribution. This approach does not reflect the natural variability of soil properties. The advanced approach models the uncertain parameters of the soil by a random field, defined not only by a probability density, but also by an auto-correlation function (or covariance function) that represents the spatial variability of the soil, due in geological hazard, by the correlation between the points of the ground. The spatial distribution of geotechnical properties in natural soil deposits is difficult to predict deterministically. Limited sampling, especially in subsurface drilling, further complicates prediction of soil properties. Prediction of the spatial occurrence of soil properties in either an optimal best estimate or within a probabilistic framework is necessary for effective numerical modeling of soils with heterogeneous properties.
Applied geostatistical estimation and simulation techniques can be used to model spatial variability from limited sample sets (or from known distributions of data). While traditional statistics generally assumes independence between samples, geostatistics take advantage of the fact that samples located in proximity to one another are often more similar than those obtained at large separation distances. Geostatistics provide a

means of quantifying this spatial correlation in soil properties and then of using that information for both estimation and stochastic simulation.

Geostatistical estimation refers to techniques that provide the best linear unbiased estimators of unknown properties. When the structural information of the data is known, then the estimator can be defined. This description requires more than the simple first-order moments of the random variable of interest. Geostatistical simulation is a spatial Monte Carlo process where a random "draw" from a local cumulative distribution function simulates a value of a property at a given location. The simulation process is run multiple times to produce a series of realizations all of which correspond to the observed data at the sample locations, the univariate distribution, and the spatial correlation of the observed data. In essence, each realization is a probable representation of the underlying reality given the available data. These multiple realizations can be used as input to a transfer function or processed to provide a map of the probability of a given situation being true (e.g., a plot of the probability that a given factor of safety will be exceeded). The results of the transfer function can often be evaluated in terms of economic loss and/or risk.

Most soils are naturally formed in many different depositional environments; therefore their physical properties will vary from point to point. This variation can exist even in an apparently homogeneous soil unit. Variability of soil properties is a major contributor to the uncertainty in geotechnical engineering analyses. Laboratory test results on natural soils indicate that most soil properties can be considered as random variables conforming to the normal distribution function

(Lumb, 1966; Tan et al., 1993).

I.3.1 Modeling parameters by random variables:

A *random variable* is a variable that can take on multiple values. The domain of a random variable is the outcome set and its range is the set of possible values. Mathematically, a random variable can be expressed as a real function, *Z(x)*, which associates a real number, *xi*, with each element in the outcome set, $x_i \in \Omega$. The real number, x_i, will correspond to every outcome of an experiment, the function

$\{Z(x) \leq x_i\}$ is an event for any real number *xi*, and the probabilities $P\{Z(x) = +\infty\}$ *and* $P\{Z(x) = -\infty\}$ will be zero for the random variable.

There are several studies [Fenton et al. (2003)] recommend a log normal law for cohesion, the Young's modulus and shear modulus, since these parameters always keep positive values. While the beta distribution is recommended for the internal friction angle and this limiting its variation in a range of practical values.

Soil parameters can be correlated. This correlation is expressed by a correlation coefficient is a statistical index that expresses the intensity and the direction of the dependence between two random variables.

I.3.2 Modeling uncertainties of soil by a random field:

The random field theory is commonly used in literature to describe the soil spatial variability. According to VanMarcke (1983), the random field theory should incorporate the observed behavior that values at adjacent locations are more related than those separated by some distance. For this purpose, a fundamental statistical property which is the autocorrelation function (ACF) is introduced in addition to the classical statistical parameters (i.e. the mean and standard deviation or coefficient of variation). The ACF is a plot of the correlation coefficient versus the distance. This ACF may be used to identify (i) the autocorrelation distance (a) or (ii) the scale of fluctuation (δ). If the soil property of interest is denoted by Z, the correlation coefficient ρ between the values of that property at two different locations is defined as follows:

$$\rho(\Delta h)=\frac{C\left[Z\left(X_i\right),Z\left(X_{i+\Delta h}\right)\right]}{\sigma_Z^2}=\frac{1}{\sigma_Z^2}E\left\{\left[Z\left(X_i\right)-\mu_Z\right]\left[Z\left(X_{i+\Delta h}\right)-\mu_Z\right]\right\} \quad \text{(I.1)}$$

Where X is the vector which represents the location. It is given by $X=(x)$ in the case of a one-dimensional random field, $X=(x,y)$ in the case of a two-dimensional (2D) random field and $X=(x,y,z)$ in the case of a three-dimensional (3D) random field. On the other hand, $Z(X_i)$ is the value of the property Z at location X_i; $Z(X_{i+\Delta h})$ is the value of the property Z at location, $X_{i+\Delta h}$; Δh is the separation distance between the data pairs; E[.] is the expected value; C is the covariance and μ_Z and σ_Z are respectively the mean and standard deviation of the property Z. It should be emphasized here that it is not possible to know the value of ρ between any two arbitrary points. Thus; in practice,

one needs to determine the ACF which allows one to calculate the value of the correlation coefficient between any two arbitrary points.

This can be done by collecting some values of the property Z (also known as the data samples) at equally separation distance Δh. These values are gathered in the vector $\chi = \{Z(X_1),...,Z(X_s)\}$ where s is the number of these data samples and $X_{i+1}=X_i + \Delta h$. These data samples are then used to determine the sample ACF as follows:

$$\rho_k = \rho(k\,\Delta h) = \frac{\sum_{i=1}^{s-k}\left[Z(X_i)-\mu_Z\right]\left[Z(X_{i+k})-\mu_Z\right]}{\sum_{i=1}^{N}\left[Z(X_i)-\mu_Z\right]^2} \qquad \text{(I.2)}$$

k=0, 1, …, K

The sample ACF is the graph of ρ_k for $k=0, 1, 2 \ldots K$, where K is the maximum allowable number of lags (data intervals). Generally, $K=s/4$ (Box and Jenkins 1970), where s is the total number of data samples.

The ACF is often used to determine the distance over which a property exhibits strong correlation. Two measures of this quantity which are the autocorrelation distance (a) or the scale of fluctuation (δ) may be evaluated. The autocorrelation distance (a) is defined as the distance required for the autocorrelation function to decay from 1 to e^{-1} (0.3679). On the other hand, the scale of fluctuation is defined as the area under the ACF [Fenton (1999)]. The determination of the autocorrelation distance (a) is done by fitting the sample ACF to one of the models given in Table I.1 where $k\Delta$h is the lag distance and (a) is the autocorrelation distance.

Model	Autocorrelation function	Scale of fluctuation (δ)
Single exponential	$\rho_k = \exp\left(\frac{-\lvert k\,\Delta h\rvert}{a}\right)$	$\delta = 2a$
Square exponential	$\rho_k = \exp\left(-\left[\frac{\lvert k\,\Delta h\rvert}{a}\right]^2\right)$	$\delta = \sqrt{\pi}a$
Cosine exponential	$\rho_k = \exp\left(-a\lvert k\,\Delta h\rvert\right)\cos\left(ak\,\Delta h\right)$	$\delta = \frac{1}{a}$
Second-order Markov	$\rho_k = \left(1+a\lvert k\,\Delta h\rvert\right)\exp\left(-a\lvert k\,\Delta h\rvert\right)$	$\delta = \frac{4}{a}$

Table I.1. Theoretical ACF used to determine the autocorrelation distance (*a*) [Vanmarcke (1983)]

Finally, it should be mentioned that the modeling of the spatial variability is greatly facilitated by the data being stationary [Uzielli et al. (2005)]. Stationarity is insured if (i) the mean is constant with distance (i.e. no trend exists in the data); (ii) the variance is constant with distance; (iii) there are no seasonal variations; and (iv) there are no irregular fluctuations. In random field theory, it is a common practice to transform a non-stationary data set to a stationary one by removing a low-order polynomial trend (i.e. a first or a second order polynomial) using the ordinary least square method.

Autocorrelation distance (a)

A literature review on the values of the autocorrelation distances of different soil types and for different soil properties was given by El-Ramly (2003) and is presented in Table I.2. It should be emphasized here that the autocorrelation function and the autocorrelation distance (*a*) are generally site specific, and often challenging due to insufficient site data and high cost of site investigations.

Test type	Soil property	Soil type	Autocorrelation distance a(m)	
			vertical	horizontal
VST	c_u(VST)	Organic soft clay	1.2	-
VST	c_u(VST)	Organic soft clay	3.1	-
VST	c_u(VST)	Sensitive clay	3.0	30.0
VST	c_u(VST)	Very soft clay	1.1	22.1
VST	c_u(VST)	Sensitive clay	2.0	-
Q_u	$c_u(Q_u)$	Chicago clay	0.4	-
Q_u	$c_u(Q_u)$	Soft clay	2.0	40.0
UU	$c_u(UU)_N$	Offshore soil	3.6	-
DSS	$c_u(DSS)_N$	Offshore soil	1.4	-
CPT	q_c	North see clay	-	30.0
CPT	q_c	Clean sand	1.6	-
CPT	q_c	North sea soil	-	13.9
CPT	q_c	North sea soil	-	37.5
CPT	q_c	Silty clay	1.0	-
CPT	q_c	Sensitive clay	2.0	-
CPT	q_c	Laminated clay	-	9.6
CPT	q_c	Dense sand	-	37.5
DMT	P_o	Varied clay	1.0	-

Table I.2. Values of the autocorrelation distances of some soil properties as given by several authors (El-Ramly 2003)

[a]VST, vane shear test; Q_u, unconfined compressive strength test; UU, unconfined undrained triaxial test; DSS, direct shear test; CPT, cone penetration test; DMT, dilatometer test;
[b]c_u(VST), undrained shear strength from VST; $c_u(Q_u)$, undrained shear strength from Q_u; $c_u(UU)_N$, normalized undrained shear strength from UU; $c_u(DSS)_N$, normalized undrained shear strength from DSS; q_c, CPT trip resistance; P_o, DMT lift-off pressure.

I.3.3 The expansion optimal linear estimation (EOLE) method for random field discretization.

The expansion optimal linear estimation method (EOLE) was proposed by Li and Der Kiureghian (1993). This method only deals with uncorrelated Gaussian random fields because it uses a spectral representation of the vector $\chi = \{Z(X_1),...,Z(X_s)\}$. To overcome the inconvenience of modeling only uncorrelated Gaussian random fields, Vořechovsky (2008) has extended this method to cover the general case of cross-correlated non-Gaussian random fields.

In this section one first presents EOLE method proposed by Li and Der Kiureghian (1993) to model uncorrelated Gaussian random fields.

In EOLE method, the fact that the spatially varying soil property is assumed to be Gaussian allows one to spectrally decompose its autocorrelation matrix $\Sigma_{\chi;\chi}$ that includes the correlation between each element of the vector $\chi = \{Z(X_1),...,Z(X_s)\}$ with all the elements of this same vector. Thus $\chi = \{Z(X_1),...,Z(X_s)\}$ can be written as follows:

$$\chi = \mu_Z + \sigma_Z \sum_{j=1}^{s} \sqrt{\lambda_j}\,\xi_j \phi_j \tag{I.3}$$

Where ξ_j ($j=1...s$) are independent standard normal random variables and (λ_j, ϕ_j) are the eigenvalues and eigenvectors of the autocorrelation matrix $\Sigma_{\chi;\chi}$ verifying $\Sigma_{\chi;\chi}\phi_j = \lambda_j \phi_j$.

The representation of the approximated random field $\tilde{Z}(X)$ is as follows:

$$\tilde{Z}(X) = \mu_Z + \sigma_Z \sum_{j=1}^{s} \frac{\xi_j}{\sqrt{\lambda_j}} \cdot \left(\phi_j\right)^T \cdot \Sigma_{Z(X);\chi} \tag{I.4}$$

where μ_Z and σ_Z are respectively the mean and the standard deviation of the Gaussian random field Z, $\Sigma_{Z(x,y);\chi}$ is the correlation vector between each element in the vector χ and the value of the field at an arbitrary point X, ξ_j is a standard normal random variable, and s is the total number of point samples.

It should be mentioned that the series expansion given in Equation (I.4) can be truncated after N<s terms. This can be done by sorting the eigenvalues λ_j in a descending order. This number N should assure that the variance of the error is smaller than a prescribed tolerance $\varepsilon \approx 10\%$. Notice that the variance of the error for EOLE is given by Sudret and Der Kiureghian (2000) as follows:

$$Var\left[Z(X) - \tilde{Z}(X) \right] = \sigma_Z^2 \left\{ 1 - \sum_{j=1}^{N} \frac{1}{\lambda_j} \left(\left(\phi_j \right)^T \Sigma_{Z(X);\chi} \right)^2 \right\} \quad \text{(I.3)}$$

Where $Z(X)$ and $\tilde{Z}(X)$ are respectively the exact and the approximate values of the random field at a given point X and $\left(\phi_j \right)^T$ is the transpose of the eigenvector ϕ_j .

I.3.4 The simulation methods

Several simulation methods are used for the uncertainty propagation. The simulation method used in this thesis is the universal Monte Carlo simulation (MCS) methodology. In spite of being rigorous and robust, the simulation methods are well-known to be very time-expensive especially when dealing with finite element or finite difference models which do not offer an analytical solution of the involved problem. The time cost is due to the fact that these methods require a great number of calls of the deterministic model to rigorously determine the PDF of the system response. Thus, the MCS methodology remains the origin of all the advanced simulation techniques.

I.3.4.1 *Monte Carlo Simulation (MCS) methodology*

The Monte Carlo simulation is a universal method to evaluate complex integrals. It consists in generating K samples which respect the joint probability density function $f_X(X)$ of the M random variables ($X_1 \ldots X_M$) gathered in a vector X. For each sample, the system response is calculated. Thus; for the K samples, one obtains K values of the system response gathered in a vector $\Gamma = \left\{ \Gamma\left(X^{(1)}\right), ..., \Gamma\left(X^{(K)}\right) \right\}$ which may be used to determine the estimators of the first two statistical moments of the system response (i.e. the mean and the standard deviation). These two estimators of the first two statistical moments ($\tilde{\mu}_\Gamma, \tilde{\sigma}_\Gamma$) are given as follows:

$$\tilde{\mu}_\Gamma = \frac{1}{K} \sum_{i=1}^{K} \Gamma\left(X^{(i)}\right) \quad \text{(I.6)}$$

$$\tilde{\sigma}_\Gamma = \frac{1}{K-1} \sum_{i=1}^{K} \left[\Gamma\left(X^{(i)}\right) - \tilde{\mu}_\Gamma \right]^2 \quad \text{(I.7)}$$

It should be mentioned here that MCS methodology is applicable whatever the complexity of the system is. However, a very large number of realizations is required to obtain a rigorous PDF of the system response. Thus, MCS methodology is not practically applicable when the deterministic model is computationally-expensive and especially when computing small failure probabilities.

I.4 The metamodeling techniques

As said previously, the simulation methods have some inconvenient, the metamodeling techniques were proposed in the purpose to overcome the inconvenience of these simulation methods. The aim of these techniques is to replace the original computationally-expensive deterministic model by a meta-model (i.e. an analytical equation).

In this thesis, we will discuss three techniques: the Polynomial Chaos Expansion (PCE), SPCE & the global sensitivity analysis (SPCE/GSA).

I.4.1 The Polynomial chaos expansion PCE methodology - the classical truncation scheme

The polynomial chaos expansion (PCE) aims at replacing a complex deterministic model (i.e. finite element/finite difference numerical model) by a meta-model. This allows one to calculate the system response (when performing MCS) using an approximate simple analytical equation [Spanos and Ghanem (1989), Isukapalli et al. (1998, 1999), Xiu and Karniadakis (2002), Berveiller et al. (2006), Huang et al. (2009), Blatman and Sudret (2010), Li et al (2011), Mollon et al. (2011), Houmadi et al. (2011), Mao et al. (2012), Al-Bittar and Soubra (2012)]. Thus, the metamodel may be used to perform the probabilistic analysis with a significant reduction in the computation time.

The PCE makes use of multivariate polynomials which are orthogonal with respect to the joint probability density function of the input random vector. The different types of the joint probability density functions and their corresponding multivariate polynomials are given in Table I..

probability density functions	Polynomials
Gaussian	Hermite
Gamma	Laguerre
Beta	Jacobi
Uniform	Legendre

Table I.3. Usual probability density functions and their corresponding families of orthogonal polynomials [Xiu and Karniadakis (2002)].

In this work, the Gaussian joint probability density function and its corresponding multivariate Hermite polynomials are used. Notice that the coefficients of the PCE may be efficiently computed using a non-intrusive technique where the deterministic calculations are done using for example a finite element or a finite difference software treated as a black box. The most used non-intrusive method is the regression approach [Isukapalli et al. (1998, 1999), Sudret et al. (2006), Huang et al. (2009), Blatman and Sudret (2010), Li et al (2011), Mollon et al. (2011), Houmadi et al. (2011), Mao et al. (2012), Al-Bittar and Soubra (2012)]. It is used in this thesis. The PCE methodology can be described as follows:

Consider a mechanical model with M input uncertain parameters gathered in a vector $X = \{X_1, \ ..., \ X_M\}$. The different elements of this vector can have different types of the probability density function. In order to represent our mechanical system response by a PCE, all the uncertain parameters should be represented by a unique chosen PDF. Table I. presents the usual probability density functions and their corresponding families of orthogonal polynomials. Based on the Gaussian PDF chosen in this work, the system response can be expanded onto an orthogonal polynomial basis as follows:

$$\Gamma_{PCE}(\xi) = \sum_{\beta=0}^{\infty} a_\beta \Psi_\beta(\xi) \cong \sum_{\beta=0}^{P-1} a_\beta \Psi_\beta(\xi) \tag{I.8}$$

where ξ is the vector resulting from the transformation of the random vector X into an independent standard normal space, P is the number of terms retained in the truncation scheme, a_β are the unknown PCE coefficients to be computed and Ψ_β are multivariate (or multidimensional) Hermite polynomials which are orthogonal with respect to the

joint probability density function of the standard normal random vector ξ. These multivariate Hermite polynomials can be obtained from the product of one-dimensional Hermite polynomials of the different random variables as follows:

$$\Psi_{\beta} = \prod_{i=1}^{M} H_{\alpha_i}(\xi) \tag{I.4}$$

Where $H_{\alpha_i}(.)$ is the α_i-th one-dimensional Hermite polynomial and α_i are a sequence of M non-negative integers $\{\alpha_1,...,\alpha_M\}$. The expressions of the one-dimensional Hermite polynomials are given in Appendix A. In practice, one should truncate the PCE representation by retaining only the multivariate polynomials of degree less than or equal to the PCE order p (i.e. the classical truncation scheme). Notice that the classical truncation scheme suggests that the first order norm $\|.\|_1$ of any multivariate polynomial Ψ_{β} should be less than or equal to the order p of the PCE as follows [Blatman (2009)]:

$$\|\alpha\|_1 = \sum_{i=1}^{M} \alpha_i \leq p \tag{I.10}$$

Using this method of truncation, the number P of unknown PCE coefficients is given by:

$$P = \frac{(M+p)!}{M!\,p!} \tag{I.11}$$

As may be seen from Equation (I.11), the number P of the PCE coefficients which is the number of terms retained in Equation (I.8) dramatically increases with the number M of random variables and the order p of the PCE. This number becomes very high in the case of random fields where the number of random variables is significant.

Once the coefficients a_{β} of the PCE given by Equation (I.8) have been computed, the statistical moments (mean, standard deviation, skewness, and kurtosis) can be calculated with no additional cost. This can be done by performing Monte Carlo simulations on the meta-model and not on the original computationally-expensive finite element/finite difference numerical model. This significantly reduces the cost of the probabilistic analysis since a large number of Monte Carlo simulations (say 1,000,000) can be performed in a negligible time when using the metamodel. The next subsection

is devoted to the method used for the computation of the coefficients a_β of the PCE using the regression approach.

Computation of the PCE coefficients by the regression approach

Consider a set of K realizations $\{\xi^{(1)} = (\xi_1,...,\xi_M),...,\xi^{(K)} = (\xi_1,...,\xi_M)\}$ of the standard normal random vector ξ. These realizations are called experimental design (ED) and can be obtained from Monte Carlo (MC) simulations or any other sampling scheme (e.g. Latin Hypercube (LH) sampling or Sobol set). We note $\Gamma = \left\{\Gamma\left(\xi^{(1)}\right),...,\Gamma\left(\xi^{(K)}\right)\right\}$, the corresponding values of the response determined by deterministic calculations. The computation of the PCE coefficients using the regression approach is performed using the following equation:

$$\widehat{a} = (\eta^T \eta)^{-1} \eta^T \Gamma \tag{I.12}$$

Where the data matrix η is defined by:

$$\eta_{i\beta} = \Psi_\beta(\xi^{(i)}), \qquad i = 1,...,K, \qquad \beta = 0,...,P-1 \tag{I.5}$$

In order to ensure the numerical stability of the treated problem in Equation (I.12), the size K of the ED must be selected in such a way that the matrix $(\eta^T \eta)^{-1}$ is well-conditioned. This implies that the rank of this matrix should be larger than or equal to the number of unknown coefficients. This test was systematically performed while solving the linear system of equations of the regression approach.

Computation of the PCE coefficient of determination

The quality of the output approximation *via* a PCE closely depends on the PCE order p. To ensure a good fit between the meta-model and the true deterministic model (i.e. to obtain the optimal PCE order), one successively increases the PCE order until a prescribed accuracy was obtained. The simplest indicator of the fit quality is the well-known coefficient of determination R^2 given by:

$$R^2 = 1 - \frac{\frac{1}{K}\sum_{i=1}^{K}\left[\Gamma\left(\xi^{(i)}\right) - \Gamma_{SPCE}\left(\xi^{(i)}\right)\right]^2}{\frac{1}{K-1}\sum_{i=1}^{K}\left[\Gamma\left(\xi^{(i)}\right) - \overline{\Gamma}\right]^2} \tag{I.14}$$

where

$$\overline{\Gamma} = \frac{1}{K}\sum_{i=1}^{K}\Gamma\left(\xi^{(i)}\right) \tag{I.15}$$

The value $R^2 = 1$ indicates a perfect fit of the true model response Γ, whereas $R^2 = 0$ indicates a nonlinear relationship between the true model response Γ and the PCE model response Γ_{PCE}. The coefficient R^2 may be a biased estimate since it does not take into account the robustness of the meta-model (i.e. its capability of correctly predicting the model response at any point which does not belong to the experimental design). As a consequence, one makes use of a more reliable and rigorous coefficient of determination denoted Q^2 [Blatman (2009)]. In order to compute this coefficient of determination Q^2, one needs to sequentially remove a point from the experiment design composed of K points. Let $\Gamma_{\xi\setminus i}$ be the meta-model that has been built from the experiment design after removing the i^{th} observation and let $\Delta^i = \Gamma(\xi^{(i)}) - \Gamma_{\xi\setminus i}(\xi^{(i)})$ be the predicted residual between the model evaluation at point $\xi^{(i)}$ and its prediction based on $\Gamma_{\xi\setminus i}$. Thus, the corresponding coefficient of determination Q^2 is obtained as follows:

$$Q^2 = 1 - \frac{\frac{1}{K}\sum_{i=1}^{K}\left(\Delta^i\right)^2}{\frac{1}{K-1}\sum_{i=1}^{K}\left[\Gamma\left(\xi^{(i)}\right) - \overline{\Gamma}\right]^2} \tag{I.16}$$

The two coefficients R^2 and Q^2 will be used in this thesis to check the accuracy of the fit.

I.4.2 Sparse Polynomial Chaos Expansion (SPCE) methodology

The polynomial chaos expansion (PCE) methodology aims at replacing a complex deterministic model whose input parameters are modeled by random variables by a meta-model which allows one to calculate the system response using an approximate analytical equation [Blatman and Sudret (2010)]. The coefficients of the PCE are computed herein using a regression approach.

For a deterministic numerical model with M input uncertain parameters, the uncertain parameters should be represented first by independent standard normal random variables $\{\xi_i\}_{i=1,\ldots,M}$ gathered in a random vector ξ. The random response Γ of our mechanical model can then be expressed by a PCE of order p fixed by the user as follows:

$$\Gamma_{PCE}(\xi) = \sum_{\beta=0}^{\infty} a_\beta \Psi_\beta(\xi) \cong \sum_{\beta=0}^{P-1} a_\beta \Psi_\beta(\xi) \tag{I.17}$$

where P is the number of terms retained in the truncation scheme, a_β are the unknown PCE coefficients to be computed and Ψ_β are multivariate (or multidimensional) Hermite polynomials which are orthogonal with respect to the joint probability distribution function of the standard normal random vector ξ. These multivariate polynomials are given by $\Psi_\beta = \prod_{i=1}^{M} H_{\alpha_i}(\xi)$, where $H_{\alpha_i}(.)$ is the α_i-th one-dimensional Hermite polynomial and α_i are a sequence of M non-negative integers $\{\alpha_1,\ldots,\alpha_M\}$. In practice, one should truncate the PCE representation by retaining only the multivariate polynomials of degree less than or equal to the PCE order p. For this reason, a classical truncation scheme based on the determination of the first order norm is generally adopted in the literature. This first order norm is defined as follows: $\|\alpha\|_1 = \sum_{i=1}^{M} \alpha_i$. The classical truncation scheme suggests that the first order norm should be less than or equal to the order p of the PCE. Using this method of truncation, the number P of the unknown PCE coefficients is given by $P = \frac{(M+p)!}{M!\,p!}$. Thus, the number P of the PCE coefficients increases dramatically with the number M of the random variables and the order p of the PCE. To overcome such a problem, it was shown that the number of

significant terms in a PCE is relatively small since the multidimensional polynomials Ψ_β corresponding to high-order interaction are associated with very small values for the coefficients a_β. Thus, a truncation strategy based on this observation was developed in which the multidimensional polynomials Ψ_β corresponding to high-order interaction were penalized. This was performed by considering the hyperbolic truncation scheme that considers the q-norm instead of the first order norm. The q-norm is given by $\|\alpha\|_q = \left(\sum_{i=1}^{M} \alpha_i^q \right)^{1/q}$ where q is a coefficient ($0<q<1$). The hyperbolic truncation scheme suggests that the q-norm should be less than or equal to the order p of the PCE. The proposed methodology leads to a SPCE that contains a small number of unknown coefficients which can be calculated from a reduced number of calls of the deterministic model. This is of particular interest in the present case of random fields which involve a significant number of random variables. This strategy will be used in this paper to build up a SPCE of the system response using an iterative procedure [Blatman and Sudret (2010)]. Once the unknown coefficients of the SPCE are determined, the PDF of the dynamic responses can be estimated using Monte Carlo technique.

I.4.3 SPCE/GSA

When dealing with high-dimensional stochastic problems making use of computationally-expensive deterministic models (e.g. three-dimensional analysis of shallow rectangular or square footings resting on 3D spatially varying ponderable soils), the time cost remains important even with the use of the SPCE. Consequently, a method that can reduce once again the cost of the probabilistic analysis (i.e. the number of calls of the deterministic model) is needed.

Dr. Al-Bittar & Dr. Soubra have proposed a combination of the SPCE methodology with the global sensitivity analysis GSA. The basic idea of this combination is that, for a given discretized random field, the obtained random variables do not have the same weight in the variability of the system response. The variables with a very small contribution in the variability of the system response can be discarded which significantly reduces the dimensionality of the treated problem. This allows one to perform a probabilistic analysis using a reduced Experiment Design (ED) and thus a

smaller number of calls of the computationally-expensive deterministic model. The main challenge remains in detecting the most influential random variables in order to reduce the dimensionality of the problem. For this purpose, a procedure that makes use of both the SPCE and the GSA (denoted hereafter by SPCE/GSA) is proposed in this regard.

A GSA based on Sobol indices is then performed on the SPCE order to determine the weight of each random variable in the variability of the system response. As a result, the variables with very small values of their Sobol indices (i.e. those that have a small weight in the variability of the system response) can be discarded. Consequently, a response which only depends on a smaller number of random variables is obtained. In other words, one obtains a response with an 'effective dimension'. This dimension is smaller than the initial dimension where the total number of random variables was considered.

The SPCE/GSA procedure can be described in more details by the following steps:

- Discretize the random field(s): This step may be made using EOLE method and its extensions by Vořechovsky. After the discretization procedure, a random field is represented by N independent standard normal random variables. If the total number of random fields involved in the analysis is equal to $N_{RF,}$ the total number of random variables is thus given by $N_T = N_{RF}xN$ which can be relatively large especially for small values of the autocorrelation distances. Notice that the equation $N_T=N_{RF}xN$ is only applicable if all the random fields share the same autocorrelation function.

- Perform a GSA based on Sobol indices to determine the weight of each random variable (of the different random fields) in the variability of the system response. The variables with very small values of their Sobol indices have no significant weight in the variability of the system response and can thus be discarded. Consequently, a response that only depends on a smaller number of random variables is obtained. In other words, one obtains a response with an 'effective dimension' N_e that is smaller than the initial dimension where the total number N_T of random variables was considered.

- Use the same Experiment Design (ED) which was employed before but this time by only keeping the most influential random variables. By reducing the number of random variables from N_T to N_e (where $N_e<N_T$), one has the possibility to use a higher SPCE order (i.e. $p>2$). The use of a higher SPCE order is necessary to lead to an improved fit of the SPCE since the coefficient of determination Q^2 increases when the SPCE order increases.

As a conclusion, the use of the SPCE/GSA procedure is expected to provide a good fit of the deterministic model with a reduced number of model evaluations as compared to the classical SPCE approach.

I.5 FLAC^{3D}

FLAC^{3D} & MATLAB are the two softwares used in this thesis.

FLAC^{3D} (Fast Lagrangian Analysis of Continua) is a computer code which allows one to perform three dimensional (3D) numerical simulations. It should be mentioned that FLAC^{3D} allows the application of stresses (stress control method) or velocities (displacement control method) on the geotechnical system. The application of stresses or velocities creates unbalanced forces in this system. The solution of a given problem in FLAC^{3D} is obtained by damping these forces to reduce them to very small values compared to the initial ones. The stresses and strains are calculated at several time intervals (called cycles) until a steady state of static equilibrium or a steady state of plastic flow is achieved in the soil mass.

It should be mentioned here that the programming language FISH in FLAC^{3D} allows one to create functions that calculates the stresses, displacements, rotations, etc. at any point in the soil mass.

FLAC^{3D} is a numerical modeling code for advanced geotechnical analysis of soil, rock, and structural support in three dimensions. FLAC^{3D} is used in analysis, testing, and design by geotechnical civil and mining engineers. It is designed to accommodate any kind of geotechnical engineering project where continuum analysis is necessary.

CHAPTER II. EFFECT OF THE SOIL SPATIAL VARIABILITY IN THREE DIMENSIONS ON THE ULTIMATE BEARING CAPACITY OF SQUARE FOUNDATIONS.

II.1 Introduction

Few authors have investigated the effect of the 3D soil spatial variability. One may cite among others Fenton and Griffiths (2005) for the foundation settlement problem, Griffiths et al. (2009) for the slope stability analysis and Popescu et al. (2005) for the seismic liquefaction problem. To the best of the authors' knowledge, there are no investigations on the effect of the 3D soil spatial variability on the ultimate bearing capacity of foundations.

The effect of the soil spatial variability in three dimensions is investigated in this chapter through the study of the ultimate bearing capacity of square foundation resting on a purely cohesive soil with a spatially varying cohesion in the three dimensions. For this purpose, the soil cohesion was modeled as a 3D random field. Both cases of isotropic and anisotropic random fields were considered.

II.2 Probabilistic analysis of square footing resting on a 3d spatially varying soil mass.

The aim of this section is to perform a probabilistic analysis of shallow foundations taking into account the soil spatial variability in three dimensions. More specifically, the analysis involves the computation of the ultimate bearing capacity (q_{ult}) of square footing resting on a purely cohesive soil that exhibits spatial variability in three dimensions.

As for the random field discretization method of the 3D random field, a straightforward extension to the 3D case of the Expansion Optimal Linear Estimation (EOLE) methodology proposed by Li and Der Kiureghian (1993) and extended by Vořechovsky (2008) was used in this chapter. It should be emphasized here that this extension of EOLE method to the 3D case is straightforward because the autocorrelation matrix $\Sigma_{\chi;\chi}$ provides the correlation between each node of the stochastic mesh and all the

nodes of this mesh. Thus, $\Sigma_{\chi;\chi}$ is always a square matrix of dimensions *sxs* regardless of the random field dimension.

Concerning the probabilistic method of analysis, the SPCE/GSA expansion method presented in the previous chapter is used herein. It aims at replacing the FLAC^{3D} deterministic model by a meta-model (i.e. a simple analytical equation). This allows one to easily calculate the system response (when performing the probabilistic analysis by MCS) using a simple analytical equation.

The deterministic model was based on numerical simulations using the finite difference code FLAC^{3D}. The undrained soil behavior was modeled using a conventional elastic-perfectly plastic model based on Tresca failure criterion. On the other hand, an associative flow rule was considered in this study. This assumption is justified by the fact that for purely cohesive materials no volume changes are expected to appear during plastic deformation. Notice that the soil Young modulus E and Poisson ratio υ were assumed to be deterministic since the ultimate bearing capacity is not sensitive to these variables. Their corresponding values were respectively $E = 60MPa$ and $\nu = 0.49$. Concerning the footing, a weightless rigid foundation was used. It was assumed to follow an elastic linear model ($E = 25GPa$, $\nu = 0.4$). The connection between the footing and the soil mass was modeled by interface elements having the same mean values of the soil shear strength parameters in order to simulate a perfectly rough soil-footing interface. These parameters have been considered as deterministic in this study. Concerning the elastic properties of the interface, they also have been considered as deterministic and their values were as follows: $K_s = 1GPa$, $K_n = 1GPa$ where K_s and K_n are respectively the shear and normal stiffnesses of the interface.

Figure II.1 shows the adopted soil domain considered in the analysis of the square footing case. It is 5mx5m wide by 2m deep. A 'relatively fine' mesh was considered for the analysis.

It should be noted that the size of a given element in the deterministic mesh depends on the autocorrelation distances of the soil properties. Der Kiureghian and Ke (1988) have suggested that the length of the largest element of the deterministic mesh in a given direction (horizontal or vertical) should not exceed 0.5 times the autocorrelation

distance in that direction. In order to respect this criterion for the different autocorrelation distances, a refinement of the deterministic mesh was performed in FLAC^{3D} for the very small values of the autocorrelation distances (<1m). This mesh will be called hereafter 'very fine' mesh.

For the boundary conditions of the square footing case, the horizontal movement on the vertical boundaries of the grid was restrained, while the base of the grid was not allowed to move in both the horizontal and the vertical directions.

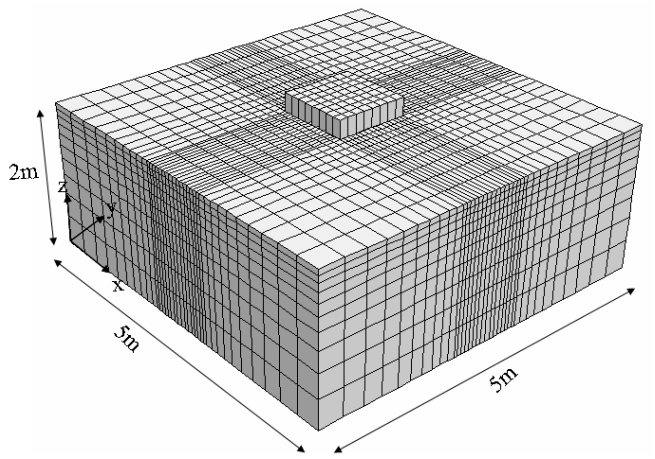

Figure II.1. Mesh used for the computation of the ultimate bearing capacity of a square footing

II.3 NUMERICAL RESULTS

In this section, one firstly presents the obtained deterministic numerical results. This is followed by a presentation of the probabilistic numerical results.

II.3.1 Deterministic numerical results

The aim of this section is to present the deterministic numerical results for the square footing considered in the analysis.

The three-dimensional 'relatively fine' mesh has led to a deterministic value of ultimate bearing capacity coefficient N_c=6.54 for the square footing case. The difference with the recent finite element solution (N_c=5.91) by Gourvenec et al. (2006) and the recent upper-bound solution (N_c=6.41) by Gourvenec et al. (2006) was respectively about 9% and 2%. It should be emphasized here that a ‘very fine’ mesh has led to a value of N_c=6.15 which is only 5% smaller (i.e. better) than the value of 6.54 obtained using the 'relatively fine' mesh. Notice however that this solution requires an increase in the

computation time by 2 hours and thus, this 'very fine' mesh was not retained in the present probabilistic analysis. A similar procedure that makes use of a 'relatively fine' (not 'very fine') mesh was advocated by Griffiths et al. (2002) when performing a probabilistic analysis. It should be emphasized herein that when dealing with probabilistic studies based on three-dimensional finite element/finite difference deterministic models, the time cost is very important especially when the soil spatial variability (and more specifically the variability of the soil property in three dimensions) is introduced. The reasons are:

(i) The computation time of a single deterministic solution significantly increases with the increase in the density of the three-dimensional deterministic mesh.

(ii) The fact of providing (for each simulation of a single probabilistic analysis) different values of the soil cohesion to the different elements of the mesh, will add a dramatic computation time especially for very fine meshes.

(iii) The large number of simulations required for each probabilistic analysis.

Thus, in order to enable the investigation of the effect of the soil spatial variability in the three dimensions for the present three-dimensional mechanical problem, a 'relatively fine' (not 'very fine') mesh was considered in the square footing case. This is a compromise between the computation time and the accuracy of the probabilistic solution.

II.3.2 Probabilistic numerical results

In this section, the probabilistic numerical results of the square footing resting on a purely cohesive spatially varying soil are presented. The soil cohesion parameter was modeled as anisotropic non-Gaussian (log-normal) random field using a square exponential autocorrelation function. Its mean value and coefficient of variation (referred to as reference values) were taken as follows: $\mu_c = 20kPa, COV_c = 25\%$.

As for the autocorrelation distances a_x, a_y and a_z of the cohesion random field, both cases of isotropic random fields (i.e. $a_x=a_y=a_z$ for the 3D random field case) and anisotropic random fields (i.e. $a_x=a_y\neq a_z$ for the 3D random field case) will be treated although the soil is rarely isotropic in reality.

When isotropic random fields are used, the autocorrelation distance will be denoted by (a) later on in this chapter (i.e. $a=a_x=a_y=a_z$ for the 3D random field case). Also, when referring to anisotropic random fields, the horizontal autocorrelation distance will be denoted by a_h (i.e. $a_h=a_x=a_y$ for the 3D random field case). Furthermore, the vertical autocorrelation distance fields will be denoted by a_v (i.e. $a_v=a_z$).

For the isotropic case, a range of 0.5-10m was considered (cf. Table II.1). For the anisotropic case, the reference values adopted for the horizontal and the vertical autocorrelation distances were 10m and 1m while the wide ranges of 0.5-10m and 0.15-10m were considered respectively for the horizontal and the vertical autocorrelation distances when performing the parametric study for the square footing (cf. Table II.1).

For the considered soil domain and for the different values of the autocorrelation distances (a, a_h *or* a_v) used in the analysis, the total number N of random variables (or eigenmodes) that should be used to discretize the cohesion random field within a value of the variance of the error $\leq 10\%$ is presented in Table II.1. It should be emphasized here, that for the very small values of the autocorrelation distance where a large number of random variables (≥ 500) was needed to discretize the random field, a maximum number of random variables N=300 was employed. This is because beyond this value, numerical difficulties may occur. The use of this number may lead to relatively large values of the variance of the error (>10%) but this will not affect the accuracy of the obtained system response. This is because of the very fast decay of the importance of random variables in the variability of the system response as was shown in the previous chapter.

		3D random field
Isotropic case with varying values of a (m)	0.5	2000
	1	500
	2	20
	5	10
	10	5
Anisotropic case with varying values of a_v (m) when a_h=10m	0.15	20
	0.25	12
	0.5	8
	1	5
	2	5
	5	5
	10	5
Anisotropic case with varying values of a_h (m) when a_v=1m	0.5	1500
	1	500
	2	30
	5	10
	10	5

Table II.1. Number of random variables needed to discretize the 3D cohesion random fields in the case of the square footing

Figure II.2 (a) presents, for the square footing, a typical realization of the 3D cohesion random field in the isotropic case where a=0.5m. Only one half of the soil domain is presented in this figure in order to show the variation of the cohesion in the plane X=2.5m (i.e. the central plan under the footing). As may be seen from this figure, dark regions correspond to small values of the cohesion c while light regions refer to lager values.

Figure II.2 (b) presents a 3D view of the failure mechanism (for the random field realization shown in Figure II.2 (a)) using the contours of the strain rate. This view clearly shows the influence of the 3D spatial variability on the obtained failure mechanism in both the central vertical plane (X=2.5m) and the top horizontal plane representing the ground surface. From this figure, one can see that the failure mechanism is more developed through the weaker zones and is limited when strong zones are encountered. Contrarily to the case of a homogeneous soil, a non-symmetrical

mechanism is obtained herein, although the footing is subjected to a symmetrical vertical load.

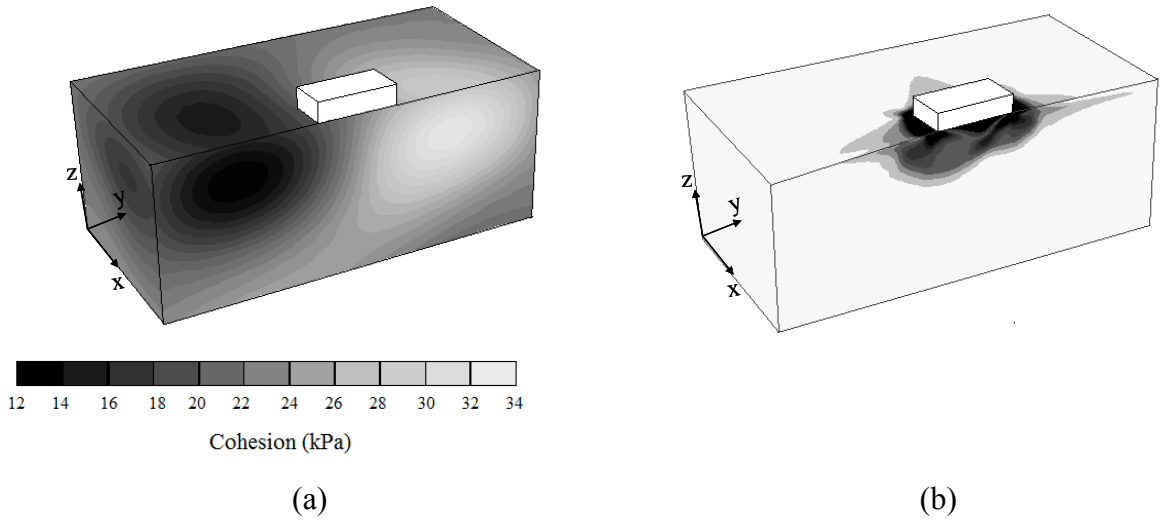

(a) (b)

Figure II.2. Perspective view of half of the soil domain showing (a) a random field realization (the contour lines provide the distribution of the soil cohesion on the envelope of this domain) and (b) the contours of the strain rate

On the other hand, the probabilistic numerical results have shown that for the particular case of a purely cohesive soil, the probabilistic ultimate bearing capacity can be written as follows: $q_{ult} = \mu_c N_c$ where μ_c is the mean value of the random field c and N_c is the probabilistic ultimate bearing capacity coefficient. This is because a change in the mean value of the random field c (for the same value of the coefficient of variation $COV_c = 25\%$) have led to the same PDF of N_c as may be seen from Figure II.3. Thus, in this chapter, the non-dimensional coefficient N_c will be used (instead of q_{ult}) to represent the ultimate bearing capacity in a probabilistic framework. This coefficient depends on the statistical parameters of the random field (i.e. autocorrelation distances and coefficient of variation). Furthermore, this coefficient (as in the deterministic analysis) is independent of the values of the soil cohesion c and the footing breadth B. It should be noted that all the probabilistic results presented in this chapter are provided for the practical value of the coefficient of variation $COV_c = 25\%$.

Finally, it should be mentioned here that for the reference case where a_h=10m and a_v=1m, the computation time is about 45 min per simulation for the square footing case. This time includes the computation of the values of the cohesion random field at the different elements centroids of the mesh and their introduction in the deterministic mesh

together with the time required for the deterministic calculation. This computation time significantly increases for the very small values of the autocorrelation distances. This is because the large number of random variables in these cases will induce additional computation time to calculate the values of the cohesion random field for the different elements centroids of the deterministic mesh. Notice finally, that for the reference case, 300 calls of the deterministic model were found to be sufficient to construct the meta-model within the prescribed target accuracy Q^2_{TARGET} =0.999.

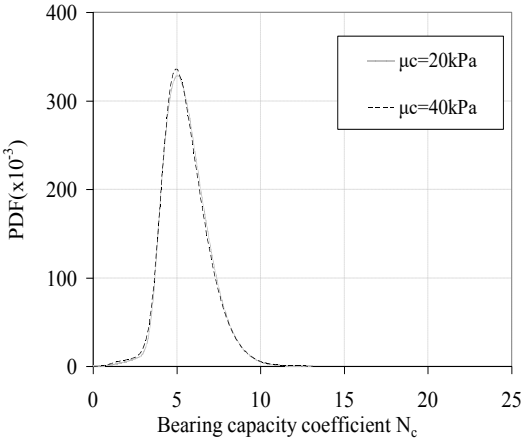

Figure II.3. Influence of the mean value of the cohesion on the PDF of the bearing capacity coefficient N_c of a strip footing when using 3D random field for a_h=10m, a_v=1m and COV_c=25%

II.3.2.1 *Effect of the autocorrelation distance: The isotropic case*

Table II.2 presents the effect of the isotropic autocorrelation distance (a) on the statistical moments of the bearing capacity coefficient N_c for the square footing using a 3D random field.

Table II.2 shows that for a small value of the autocorrelation distance (a=0.5m), the variability of the bearing capacity coefficient (expressed by the non-dimensional parameter COV_{N_c}) is smaller when a 3D random field is considered. However, for the large values of the autocorrelation distance (a=10m), quasi-similar values of the response variability were obtained in the case of 3D random field. These observations are valid for the square footing.

Table II.2 also shows that for the square footing, the variability of N_c decreases when the autocorrelation distance decreases. For the very large values of the autocorrelation distance, the 3D random field is superimposed because it tends to its limiting case of

random variable for which the autocorrelation distance is infinite. The decrease in the autocorrelation distance from infinity to a finite value (moderate or small where $a \leq 5m$) limits the correlation (in a given simulation) to a finite zone which leads to a smaller variability in the system response.

		Square footing		
	a (m)	μ_{N_c}	σ_{N_c}	COV_{N_c} (%)
3D random field	0.5	6.34	0.51	8.0
	1	6.39	1.02	15.9
	2	6.46	1.38	21.3
	5	6.51	1.53	23.5
	10	6.52	1.58	24.2

Table II.2. Effect of the isotropic autocorrelation distance (a) on the statistical moments μ_{N_c} and σ_{N_c} of the bearing capacity coefficient N_c of square footing using 3D random field

II.3.2.2 *Effect of the autocorrelation distance: The anisotropic case*

Table II.3 presents the effect of the vertical autocorrelation distance a_v on the statistical moments of the bearing capacity coefficient N_c for the square footing using 3D random field when a_h=10m. Similarly, Table II.4 presents the effect of the horizontal autocorrelation distance a_h on the statistical moments of the bearing capacity coefficient N_c for the square footing using 3D random field when a_v=1m.

		Square footing		
	a_v (m)	μ_{N_c}	σ_{N_c}	COV_{N_c} (%)
3D random field	0.15	6.24	0.96	15.3
	0.25	6.27	1.15	18.3
	0.5	6.38	1.38	21.7
	1	6.48	1.52	23.5
	2	6.51	1.57	24.1
	5	6.51	1.58	24.2
	10	6.52	1.58	24.2

Table II.3. Effect of the vertical autocorrelation distance (a_v) on the statistical moments μ_{N_c} and σ_{N_c} of the bearing capacity coefficient N_c of square footing using 3D random field

		Square footing		
	a_h (m)	μ_{N_c}	σ_{N_c}	COV_{N_c} (%)
3D random field	0.5	6.34	0.48	7.6
	1	6.39	1.02	15.9
	2	6.44	1.32	20.4
	5	6.46	1.48	22.9
	10	6.48	1.52	23.5

Table II.4. Effect of the horizontal autocorrelation distance (a_h) on the statistical moments μ_{N_c} and σ_{N_c} of the bearing capacity coefficient N_c of square footing using 3D random field

Table II.3 and Table II.4 also show that for the square footing, the variability of N_c decreases when the autocorrelation distance decreases. This can be explained by the fact that for the very large values of the horizontal autocorrelation distance a_h (a_h=10m), the 3D random field tends to its limiting case of a one-dimensional random field with a vertically varying soil mass. Similarly, for the very large values of the vertical autocorrelation distance a_v (a_v=10m), the 3D random field tends respectively to its limiting cases of one- and two-dimensional random fields with a horizontally varying soil masses. In all these cases, the cohesion random field is perfectly correlated in a prescribed direction (horizontal or vertical); however, the other direction (vertical or horizontal) is allowed to exhibit variations in the value of the cohesion according to the value of the autocorrelation distance fixed for that direction. This induces a reduction in the variability of N_c with respect to the case where a_h=a_v=10m. The decrease in the autocorrelation distance from the case of a horizontally varying soil mass (where $a_v = \infty$) or a vertically varying soil mass (where $a_h = \infty$) to the case where the infinite value of the autocorrelation distance decreases to a finite value, re-create further variations in the value of the cohesion. This reduces once again the variability of N_c with respect to the case where a_h=a_v=10m.

CHAPTER III. EFFECT OF THE SOIL SPATIAL VARIABILITY IN THREE DIMENSIONS ON THE ULTIMATE BEARING CAPACITY OF RECTANGULAR FOUNDATIONS.

III.1 Introduction

In this chapter, an extension of the square footing to a rectangular footing will be done in order to compare the results between the two types of foundations.

The effect of the soil spatial variability in three dimensions is investigated in this chapter through the study of the ultimate bearing capacity of rectangular foundation resting on a purely cohesive soil with a spatially varying cohesion in the three dimensions. For this purpose, the soil cohesion was modeled as a 3D random field. Both cases of isotropic and anisotropic random fields were considered.

III.2 Probabilistic analysis of square footing resting on a 3d spatially varying soil mass.

The aim of this section is to perform a probabilistic analysis of shallow foundations taking into account the soil spatial variability in three dimensions. More specifically, the analysis involves the computation of the ultimate bearing capacity (q_{ult}) of rectangular footing resting on a purely cohesive soil that exhibits spatial variability in three dimensions.

Concerning the probabilistic method of analysis, the SPCE/GSA expansion method chapter is used herein.

The deterministic model was based on numerical simulations using the finite difference code FLAC^{3D}. The undrained soil behavior was modeled using a conventional elastic-perfectly plastic model based on Tresca failure criterion. On the other hand, an associative flow rule was considered in this study. This assumption is justified by the fact that for purely cohesive materials no volume changes are expected to appear during plastic deformation. Notice that the soil Young modulus E and Poisson ratio υ were

assumed to be deterministic since the ultimate bearing capacity is not sensitive to these variables. Their corresponding values were respectively $E = 60MPa$ and $\nu = 0.3$.

Concerning the footing, a weightless rigid foundation was used. It was assumed to follow an elastic linear model ($E = 25GPa$, $\nu = 0.4$). The connection between the footing and the soil mass was modeled by interface elements having the same mean values of the soil shear strength parameters in order to simulate a perfectly rough soil-footing interface. These parameters have been considered as deterministic in this study. Concerning the elastic properties of the interface, they also have been considered as deterministic and their values were as follows: $K_s = 1GPa$, $K_n = 1GPa$ where K_s and K_n are respectively the shear and normal stiffnesses of the interface.

Figure II.1 shows the adopted soil domain considered in the analysis of the square footing case. It is 6mx9m wide by 4m deep. A 'relatively fine' mesh was considered for the analysis.

For the boundary conditions of the rectangular footing case, the horizontal movement on the vertical boundaries of the grid was restrained, while the base of the grid was not allowed to move in both the horizontal and the vertical directions.

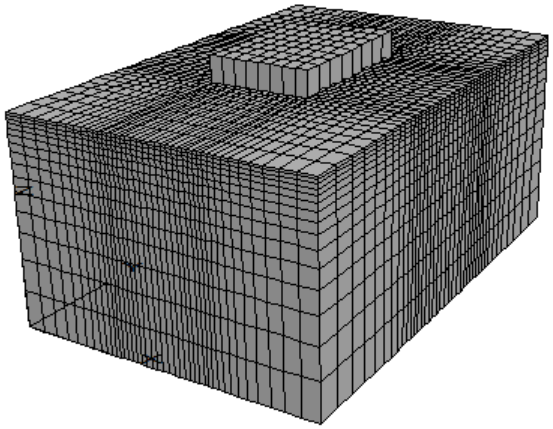

Figure III.1. Mesh used for the computation of the ultimate bearing capacity of a rectangular footing

III.3 NUMERICAL RESULTS

In this section, one firstly presents the obtained deterministic numerical results. This is followed by a presentation of the probabilistic numerical results.

III.3.1 Deterministic numerical results

The aim of this section is to present the deterministic numerical results for the rectangular footing considered in the analysis.

The three-dimensional 'relatively fine' mesh has led to a deterministic value of ultimate bearing capacity coefficient N_c=6.203 for the rectangular footing case.

III.3.2 Probabilistic numerical results

In this section, the probabilistic numerical results of the rectangular footing resting on a purely cohesive spatially varying soil are presented. The soil cohesion parameter was modeled as anisotropic non-Gaussian (log-normal) random field using a square exponential autocorrelation function. Its mean value and coefficient of variation (referred to as reference values) were taken as follows: $\mu_c = 20kPa, COV_c = 25\%$.

As for the autocorrelation distances a_x, a_y and a_z of the cohesion random field, both cases of isotropic random fields (i.e. a_x=a_y=a_z for the 3D random field case) and anisotropic random fields (i.e. a_x=a_y≠a_z for the 3D random field case) will be treated although the soil is rarely isotropic in reality.

When isotropic random fields are used, the autocorrelation distance will be denoted by (a) later on in this chapter (i.e. a=a_x=a_y=a_z for the 3D random field case). Also, when referring to anisotropic random fields, the horizontal autocorrelation distance will be denoted by a_h (i.e. a_h=a_x=a_y for the 3D random field case). Furthermore, the vertical autocorrelation distance fields will be denoted by a_v (i.e. a_v=a_z).

For the isotropic case, a range of 0.25-30m was considered (cf. Table II.). For the anisotropic case, the reference values adopted for the horizontal and the vertical autocorrelation distances were 12m and 1m while the wide ranges of 0.25-12m and 1-

15m were considered respectively for the horizontal and the vertical autocorrelation distances when performing the parametric study for the rectangular footing (cf. Table III.1).

		3D random field
Isotropic case with varying values of a (m)	0.25	4000
	0.5	2000
	1	255
	2	46
	4	10
	6	4
	9	2
	12	2
	15	2
	30	2
Anisotropic case with varying values of a_v (m) when a_h=12m	0.25	26
	0.5	14
	1	5
	2	4
	4	3
	8	2
	12	2
Anisotropic case with varying values of a_h (m) when a_v=1m	1	255
	2	81
	3	41
	6	16
	9	9
	12	5
	15	5

Table III.1. Number of random variables needed to discretize the 3D cohesion random fields in the case of the rectangular footing.

It should be mentioned here that not all cases of different autocorrelation distances were treated, that is due to the very long computation time needed for the very small values of the autocorrelation distance and the obligation to finish the project at the specified time.

Figure III.2 (a) presents, for the rectangular footing, a typical realization of the 3D cohesion random field in the anisotropic case where a_h=9m and a_v=1m. As may be seen from this figure, dark regions correspond to small values of the cohesion *c* while light regions refer to lager values.

Figure III.2 (b) presents a 3D view of the failure mechanism (for the random field realization shown in Figure III.2 (a)) using the contours of the strain rate. This view clearly shows the influence of the 3D spatial variability on the obtained failure mechanism from this figure, one can see that the failure mechanism is more developed through the weaker zones and is limited when strong zones are encountered.

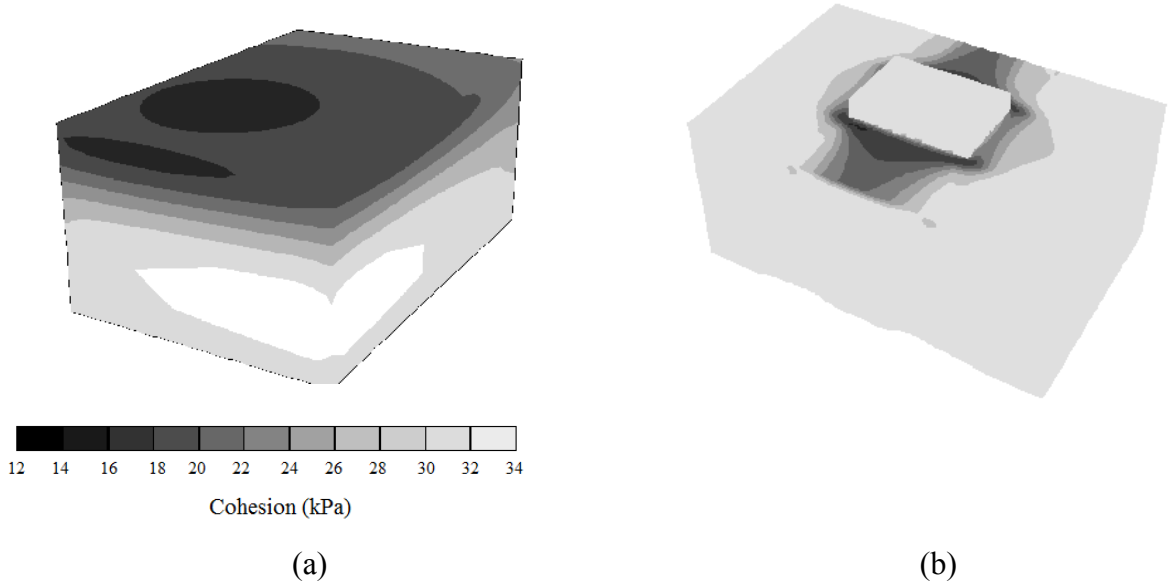

Figure III.2. Perspective view of the soil domain showing (a) a random field realization (the contour lines provide the distribution of the soil cohesion on the envelope of this domain) and (b) the contours of the strain rate

On the other hand, the probabilistic numerical results have shown that for the particular case of a purely cohesive soil, the probabilistic ultimate bearing capacity can be written as follows: $q_{ult} = \mu_c N_c$ where μ_c is the mean value of the random field *c* and N_c is the probabilistic ultimate bearing capacity coefficient. This is because a change in the mean value of the random field *c* (for the same value of the coefficient of variation $COV_c = 25\%$) have led to the same PDF of N_c as may be seen from Figure II.3. Thus, in this chapter, the non-dimensional coefficient N_c will be used (instead of q_{ult}) to

represent the ultimate bearing capacity in a probabilistic framework. This coefficient depends on the statistical parameters of the random field (i.e. autocorrelation distances and coefficient of variation). Furthermore, this coefficient (as in the deterministic analysis) is independent of the values of the soil cohesion c and the footing breadth B. It should be noted that all the probabilistic results presented in this chapter are provided for the practical value of the coefficient of variation $COV_c = 25\%$.

Finally, it should be mentioned here that for the reference case where a_h=9m and a_v=1m, the computation time is about 65 min per simulation for the rectangular footing case. This time includes the computation of the values of the cohesion random field at the different elements centroids of the mesh and their introduction in the deterministic mesh together with the time required for the deterministic calculation. This computation time significantly increases for the very small values of the autocorrelation distances. This is because the large number of random variables in these cases will induce additional computation time to calculate the values of the cohesion random field for the different elements centroids of the deterministic mesh. Notice finally, that for the reference case, 300 calls of the deterministic model were found to be sufficient to construct the meta-model within the prescribed target accuracy Q^2_{TARGET} =0.9989.

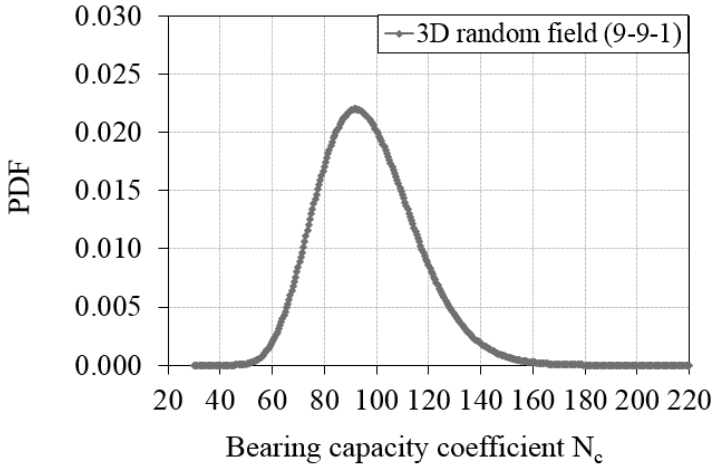

Figure III.3. PDF of the bearing capacity coefficient N_c of a rectangular footing when using 3D random field for a_h=9m, a_v=1m and COV_c=25%

III.3.2.1 *Effect of the autocorrelation distance: The isotropic case*

Table III.2 presents the effect of the isotropic autocorrelation distance (a) on the statistical moments of the bearing capacity coefficient N_c for the square footing using a 3D random field.

Table III.2 also shows that for the rectangular footing, the variability of N_c decreases when the autocorrelation distance decreases. For the very large values of the autocorrelation distance, the 3D random field is superimposed because it tends to its limiting case of random variable for which the autocorrelation distance is infinite. The decrease in the autocorrelation distance from infinity to a finite value (moderate or small where $a \leq 5m$) limits the correlation (in a given simulation) to a finite zone which leads to a smaller variability in the system response.

	Rectangular footing			
3D random field	a (m)	μ_{N_c}	σ_{N_c}	COV_{N_c} (%)
	4	4.92	0.97	19.73
	12	5.02	1.1825	23.74
	15	5.76	1.2	26.04

Table III.2. Effect of the isotropic autocorrelation distance (a) on the statistical moments μ_{N_c} and σ_{N_c} of the bearing capacity coefficient N_c of rectangular footing using 3D random field

III.3.2.2 *Effect of the autocorrelation distance: The anisotropic case*

Table III.3 presents the effect of the vertical autocorrelation distance a_v on the statistical moments of the bearing capacity coefficient N_c for the rectangular footing using 3D random field when a_h=12m. Similarly, Table III.4 presents the effect of the horizontal autocorrelation distance a_h on the statistical moments of the bearing capacity coefficient N_c for the rectangular footing using 3D random field when a_v=1m.

		Rectangular footing		
3D random field	a_v (m)	μ_{N_c}	σ_{N_c}	COV_{N_c} (%)
	2	4.94	1.08	21.86
	8	4.97	1.16	23.34
	12	5.02	1.18	23.5

Table III.3. Effect of the vertical autocorrelation distance (a_v) on the statistical moments μ_{N_c} and σ_{N_c} of the bearing capacity coefficient N_c of rectangular footing using 3D random field

		Rectangular footing		
3D random field	a_h (m)	μ_{N_c}	σ_{N_c}	COV_{N_c} (%)
	6	4.84	0.8	16.52
	9	4.86	0.92	18.93
	15	4.93	0.94	19.07

Table III.4. Effect of the horizontal autocorrelation distance (a_h) on the statistical moments μ_{N_c} and σ_{N_c} of the bearing capacity coefficient N_c of rectangular footing using 3D random field

Table III.3 and Table III.4 also show that for the rectangular footing, the variability of N_c decreases when the autocorrelation distance decreases. This can be explained by the fact that for the very large values of the horizontal autocorrelation distance a_h (a_h=12m), the 3D random field tends to its limiting case of a one-dimensional random field with a vertically varying soil mass. Similarly, for the very large values of the vertical autocorrelation distance a_v (a_v=12m), the 3D random field tends respectively to its limiting cases of one- and two-dimensional random fields with a horizontally varying soil masses. In all these cases, the cohesion random field is perfectly correlated in a prescribed direction (horizontal or vertical); however, the other direction (vertical or horizontal) is allowed to exhibit variations in the value of the cohesion according to the value of the autocorrelation distance fixed for that direction. This induces a reduction in the variability of N_c with respect to the case where a_h=a_v=12m. The decrease in the autocorrelation distance from the case of a horizontally varying soil mass (where $a_v = \infty$) or a vertically varying soil mass (where $a_h = \infty$) to the case where the infinite value of the autocorrelation distance decreases to a finite value, re-create further variations in the value of the cohesion. This reduces once again the variability of N_c with respect to the case where a_h=a_v=12m.

III.3.3 Discussion

A comparison between the values of the coefficients of variation of N_c for both the isotropic and anisotropic cases and for the square and rectangular footings is provided in Table III.5. This comparison is presented in the form of a ratio between the values of the coefficients of variation of the 3D random field.

Due to the lack of information obtained from calculation cases, a clear comparison could not be done herein, so we can satisfy by these comparison values that show that this ratio is not so much bigger than 1 in the cases presented below. This can lead to a conclusion that either in the case of square footing or rectangular footing, the values of the ultimate bearing capacity do not change in a big range between the two cases. We can also deduce that the autocorrelation distance has an important effect on the values of the ultimate bearing capacity.

Autocorrelation distance (m)	Values of $COV_{Nc}^{square}/COV_{Nc}^{rectangular}$ for different values of the isotropic autocorrelation distance	Values of $COV_{Nc}^{square}/COV_{Nc}^{rectangular}$ for different values of the vertical autocorrelation distance a_v	Values of $COV_{Nc}^{square}/COV_{Nc}^{rectangular}$ for different values of the horizontal autocorrelation distance a_h when a_v=1m
2	-	1.1	-
4	1.08	1.03	1.38
12	1.02	1.03	1.24
15	-	-	-

Table III.5. Ratios between the coefficients of variation values of N_c (obtained using 3D random field) for the square footing

III.4 Conclusions

A probabilistic analysis that considers the effect of the spatial variability in three dimensions was investigated through the study of the ultimate bearing capacity of square and rectangular foundations resting on a purely cohesive soil with a spatially varying cohesion in the three dimensions. The main reason for which a purely cohesive soil was used is to investigate the effect of the spatial variability in the third direction with the use of a relatively non-expensive deterministic model .

The soil cohesion parameter was modeled as anisotropic non-Gaussian (log-normal) random field with a square exponential autocorrelation function. A straightforward extension to the 3D case of the Expansion Optimal Linear Estimation (EOLE) methodology proposed by Li and Der Kiureghian (1993) and extended by Vořechovsky (2008) was used in this chapter. The deterministic model was based on 3D numerical simulations using FLAC3D software. An efficient uncertainty propagation methodology that makes use of a non-intrusive approach to build up a sparse polynomial chaos expansion for the system response was employed .

The probabilistic numerical results have shown that for small values of the autocorrelation distances, the variability of the ultimate bearing capacity computed by considering a 3D random field is smaller than that of the bigger values of the autocorrelation distance for square and rectangular footings.

CHAPTER IV. BUILDING DESIGN

IV.1 Introduction

This chapter resumes the design of the main constructive elements in a building. The procedure followed in this chapter is first, analyzing the building on ETABS software, getting the loads table on each element to be designed later on using s-concrete software for columns and shear walls and SAFE for the design of the slab and the raft foundation.

IV.2 Description of the project

The project is composed of two blocks, we choose to design one of them like an independent building.

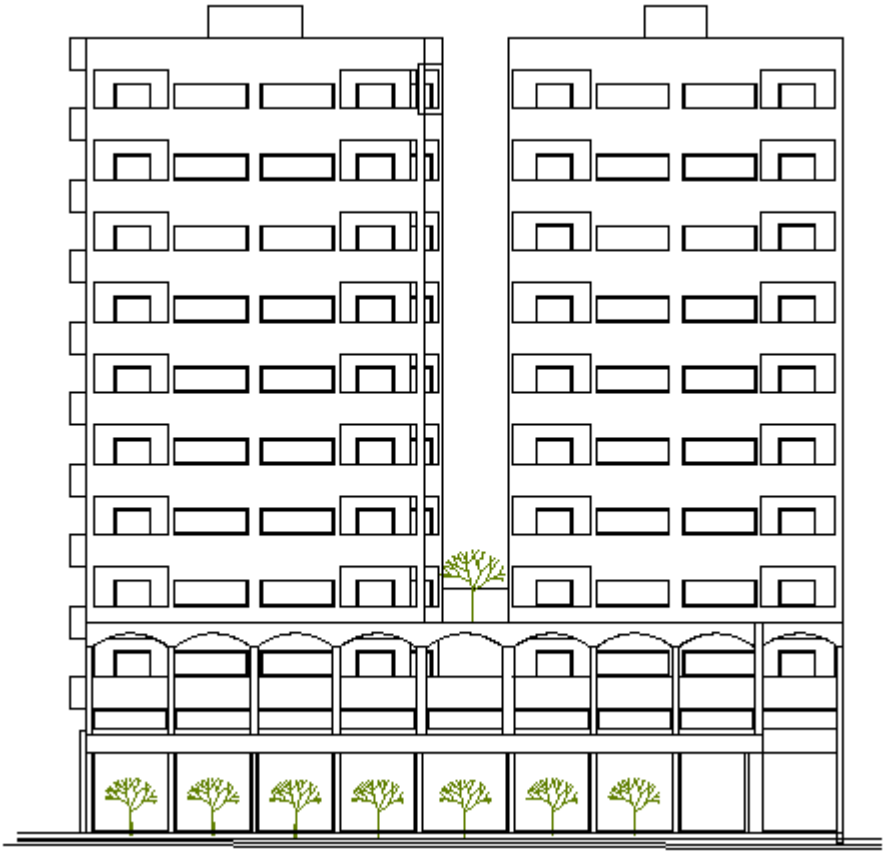

Figure IV.1. Building front elevation

The building to design is a simple residential building located in Abu-Samra, north Lebanon. This building is composed of 9 storeys and shops with their mezzanines in the ground floor.

IV.2.1 Plans description

Every story consists of two apartments 114 m^2 and is 3m height. The total area of each floor plan is 230 m^2.

The height of the shops is 3.2m and the mezzanine's is 2.5m.

- The core wall of the tower has 1 elevator and 1 staircase serving all stories.
- The basement consists of:
  - Stores for the shops.
  - 6 parking spaces belonging to the stores.
- The ground floor consists of:
  - 32 parking spaces for all apartments of both buildings.
  - 2 Guard rooms.
  - Mechanical and electrical technical rooms.
  - 1 ramp.

The following figure shows the ground floor plan:

Figure IV.2. Ground floor plan

The mezzanine story plan is as follows:

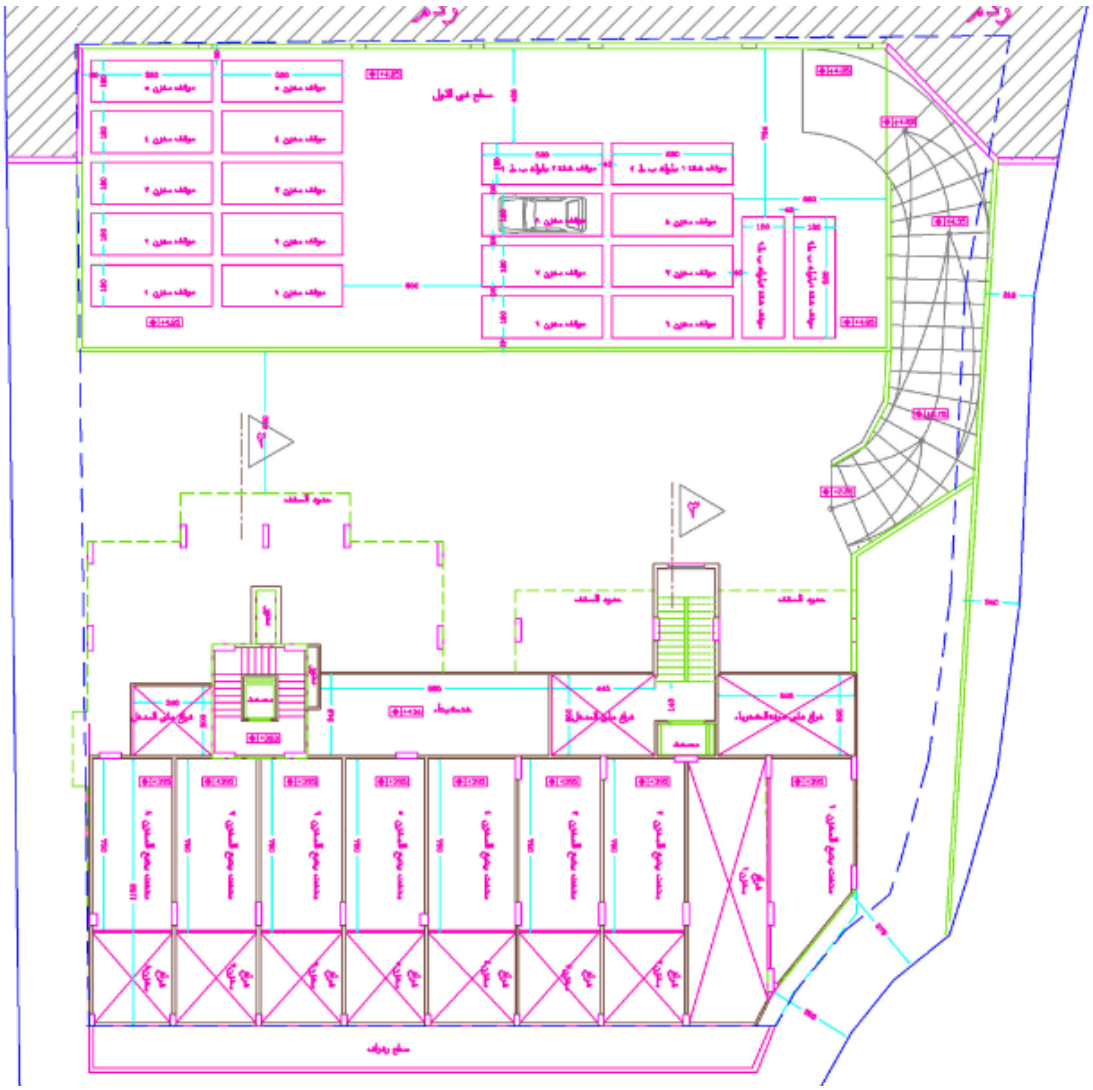

Figure IV.3. Mezzanine story plan

The repetitive story plan is shown in the next figure:

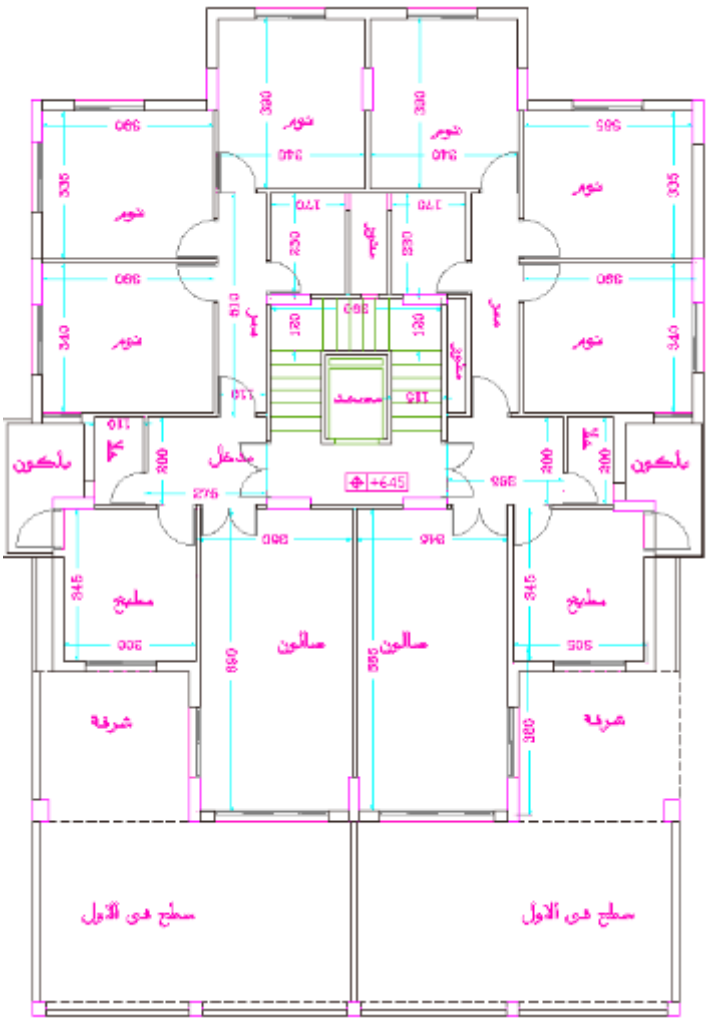

Figure IV.4. Repetitive story plan

The total area of a floor plan is 230 m^2. Each apartment is composed of 3 bed rooms, a salon, a kitchen and two toilets.

No architectural modifications were made for any of the floor plans.

IV.2.2 Lateral elevation

No architectural modifications were made to the lateral elevation of this building.

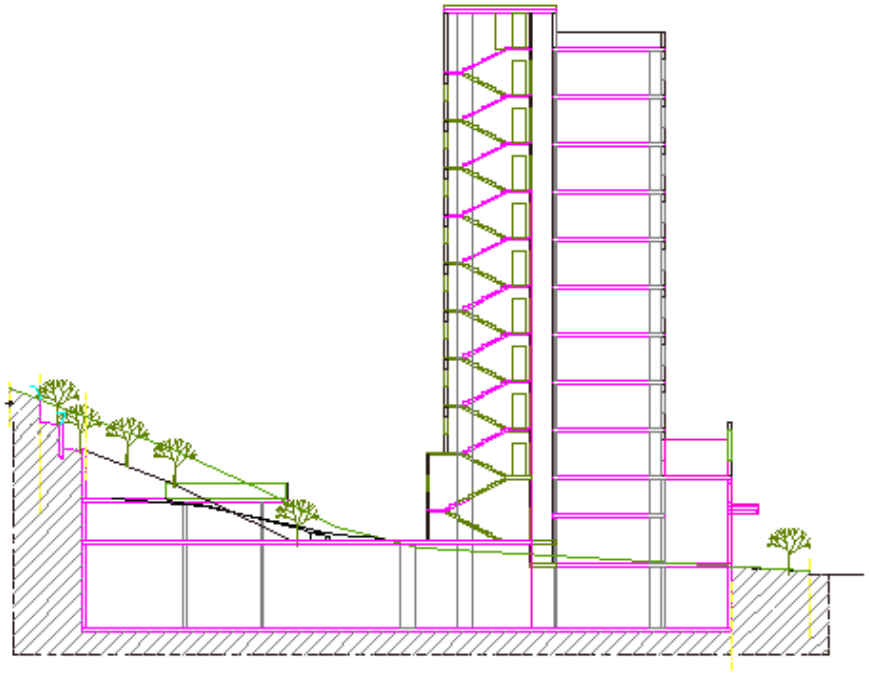

Figure IV.5. Vertical cut section of the building

IV.3 Structural design and design criteria

In this part, we will give a general view on loadings and combinations that should be used in the design of the building and present all softwares used to do a full design of the building.

IV.3.1 Loadings

A structure, or a part of it, is considered to be failed once it reaches one of the various limit states. The considered states are:

- Ultimate limit state (ULS): this state refers to loads that could lead to structural failure, human damages, serious financial losses…. Here the probability of failure must be low, that's why we increase the loading by factors.
- Serviceability limit state (SLS): this state refers to the criteria of ensuring an elastic behavior of the structure under normal working conditions.

The designed loads to be considered in accordance to the **ACI 318-05** standard code are estimated as:

- **Dead loads:**
  - Self-weight of the structural elements based on preliminary dimensioning of the structural sections and the material specific unit weight.
  - Super imposed dead loads including finishing and allowance for partitions: 5 KN/m^2 for all stories (2 KN/m^2 for partitions and 3 KN/m^2 for finishes).
- **Live loads:**
  - For current stories and ground level: 3.5 KN/m^2.
  - For the roof: 0.25 KN/m^2.
- **Seismic loads:**

The seismic loads are calculated from the story mass distribution over the structure using code-dependent coefficients and fundamental periods of vibration. For semi-rigid floor systems where there are numerous mass points, ETABS has a special load dependent Ritz-vector algorithm for fast automatic calculation of the predominant time periods.

The seismic loads are applied at the locations where the inertia forces are generated and do not have to be at story levels only. Additionally, for semi-rigid floor systems, the inertia loads are spatially distributed across the horizontal extent of the floor in proportion to the mass distribution, thereby accurately capturing the shear forces generated across the floor diaphragms.

ETABS also has a very wide variety of Dynamic Analysis options, varying from basic response spectrum analysis to nonlinear time history analysis. Code-dependent response spectrum curves are built into the system, and transitioning to a dynamic analysis is usually trivial after the basic model has been created.

In the case of this project the earthquake input data are the following:

Earthquake input data	
Period calculation coefficient Ct	Ct=0.02
Soil profile type	Sc (very dense soil profile and sot rock)
Seismic zone factor	Z=0.3
Over strength factor R	R=8.5
Importance factor I	I=1
Seismic coefficient Cv	Cv=0.45
Seismic coefficient Ca	Ca=0.33

Table IV.1. Earthquake input data

a) **Static analysis:**

For the static approach analysis of the seismic forces we have to define two seismic cases of loadings: EQX and EQY with an accidental eccentricity equal to 5% of the building projected length to the earthquake directions.

b) **Dynamic analysis:**

For the dynamic approach analysis of the seismic forces we have to define two response spectrum cases: SPECX and SPECY with a damping ratio equal to 0.05.

IV.3.2 Design criteria

IV.3.2.1 Softwares:

- **AutoCAD**: Used for architectural drawings, design drawings, and explicative drawing in the project.
- **Microsoft office**: Used for the preparation of the project's report and presentation.
- **ETABS (Extended Three dimensional Analysis of Building System):** Used for the modeling of the structure, design of vertical elements (Columns, Shear Walls…).

- **SAFE 12 (Slab Analysis by Finite Element method)**: Used for the design of horizontal elements (slabs, beams, rafts…).
- **S-CONCRETE**: Used for the design of beams, columns as well as shear walls. This software computes two types of strength utilizations: Shear and torsion utilization; axial load and moment (N vs. M) utilization. The utilization equals the applied force or moment divided by the capacity of the section.

IV.3.2.2 Design codes

- **ACI 315-05**: Used for the determination of loads combinations, the design and detailing of various concrete elements (slabs, columns and walls).
- **The Uniform Building Code "UBC 97"**: Used for the determination of lateral forces intensity and distribution (Earthquake).
- **The ASCE 7-02**: Used for the determination of lateral forces intensity and distribution (Wind).

IV.3.2.3 Material of construction

- Concrete compressive strength:
  - Shear walls, Columns: f'c = 30 MPa and E_C= 28000 MPa.
  - Slabs: f'c = 25 MPa and E_C = 25000 MPa.
- Reinforcing steel:
  - Yield strength of tensile steel reinforcement: f_y = 400 MPa.
  - Yield strength of shear reinforcement: f_y = 240 MPa.
  - Modulus of elasticity of steel: E_S = 200000 MPa.

IV.4 Model on Etabs

IV.4.1 Etabs data input

ETABS (***E**xtended **T**hree dimensional **A**nalysis of **B**uilding **System)*** is the solution, whether you are designing a simple 2D frame or performing a dynamic analysis of a complex high-rise that utilizes non-linear dampers for inter-story drift control.

ETABS has long been a favorite for the analysis and design of buildings, and whether the project is a one story shopping center or the tallest building in the world, this latest release offers the comprehensive tools needed to produce timely, efficient and elegant engineering solutions.

IV.4.1.1 DXF plan

In the DXF floor plan, walls are designated by lines, columns are designated by a cross referring to their center and axis are drawn by center line. We move the position of the columns in order to put many them on a same axis only if the distance to be moved is less than 50cm otherwise, we draw a new axis for these columns. This DXF file will be imported later on ETABS in order to make a special analysis leading at the end to make the design vertical structural elements.

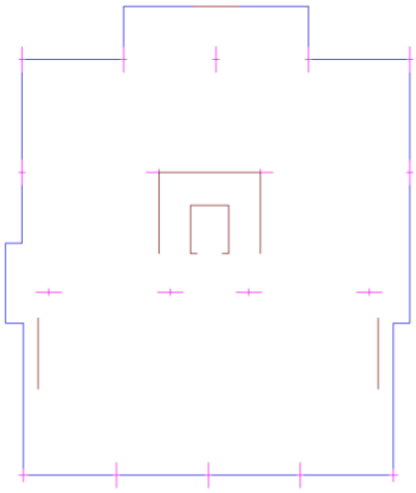

Figure IV.6. DXF floor plan of repetitive story

IV.4.1.2 Materials

- Concrete compressive strength for columns, slabs & beams: f'c = 25 MPa.
- Concrete compressive strength for walls: f'c = 30 MPa.
- Steel reinforcements yield stress f_y = 400 MPa.

IV.4.1.3 Loadings

CASE	TYPE	Auto Lateral Load	SW multiplier
DEAD	DEAD		1
SDL	SUPER DEAD		0
LIVE	LIVE		0
EQX	QUAKE	UBC 97	0
EQY	QUAKE	UBC 97	0

WINDX	WIND	ASCE 7-10	0
WINDY	WIND	ASCE 7-10	0

Table IV.2. Static load cases

- **Dead load**: self-weight (automatically taken by ETABS; it is function of the sections of the structural elements).
- **Super imposed dead load (SIDL):** include finishing and allowance for partitions: 5 KN/m^2 in all stories (2 KN/m^2 for partitions and 3 KN/m^2 for finishes).
- **Live load (LL):**
  - For basement: 5 KN/m^2
  - For all other plans: 3 KN/m^2

The corresponding masses of loads that participate in the mass source for the seismic design are: Dead load and Super imposed dead load (SIDL) with coefficient multiplier equal to 1 for each case.

- **EQX**: earthquake static load in X direction calculated according to UBC 97 with a minimum eccentricity of 5 % as specified by the seismic code.
- **EQY**: earthquake static load in Y direction calculated according to UBC 97 with a positive minimum eccentricity of 5 % as specified by the seismic code.
- **WINDX**: wind static load in X direction calculated according to ASCE 7-02. We should note that we take the gust factor in X direction equal 0.85 (stiff building).
- **WINDY**: wind static load in Y direction calculated according to ASCE 7-02. We should note that we take the gust factor in Y direction equal 0.85 (stiff building)

For the seismic dynamic analysis two response spectrums are defined: SPECX and SPECY with a damping ratio of 5%, and an eccentricity ratio of 0.05.

As we have an irregular shape the results should be scaled by the ratio

$$r = \frac{Vstatic}{Vdynamic}$$

$$r_x = \frac{168.7894}{168.7894} = 1.002$$

$$r_y = \frac{122.8235}{118.7579} = 1.034$$

IV.4.1.4 Load combinations

We will have 2 files to study the building under loads:

- Elastic analysis considering the service combinations and checking the displacement and period of the building that must be under the critical ones,
- And plastic analysis considering the ultimate combinations and designing all elements under the envelope loads.

Name	DEAD	SDL	LIVE	EQXP	EQYP	WINDX	WINDY
COMB1	1.2	1.2	1.6	-	-	-	-
COMB2	1.2	1.2	1	1	0.3	-	-
COMB3	1.2	1.2	1	0.3	1	-	-
COMB4	1.2	1.2	1	-	-	1.6	-
COMB5	1.2	1.2	1	-	-	-1.6	-
COMB6	1.2	1.2	1	-	-	-	1.6
COMB7	1.2	1.2	1	-	-	-	-1.6
COMB8	0.9	0.9	0.9	-	-	1.6	-
COMB9	0.9	0.9	0.9	-	-	-1.6	-
COMB10	0.9	0.9	0.9	-	-	-	1.6
COMB11	0.9	0.9	0.9	-	-	-	-1.6
COMB12	0.9	0.9	0.9	1	0.3	-	-
COMB13	0.9	0.9	0.9	0.3	1	-	-

Table IV.3. Load combinations

IV.4.2 Story data

Story	Height (m)	Elevation (m)	Similar to
Roof	3	36	None
Story 11	3	33	Story 1
Story 10	3	30	Story 1
Story 9	3	27	Story 1
Story 8	3	24	Story 1

Story 7	3	21	Story 1
Story 6	3	18	Story 1
Story 5	3	15	Story 1
Story 4	3	12	Story 1
Story 3	3	9	Story 1
Story 2	3	6	Story 1
Story 1	3	3	Story 1

Table IV.4. Story data

IV.4.3 Etabs output views

IV.4.3.1 3D view

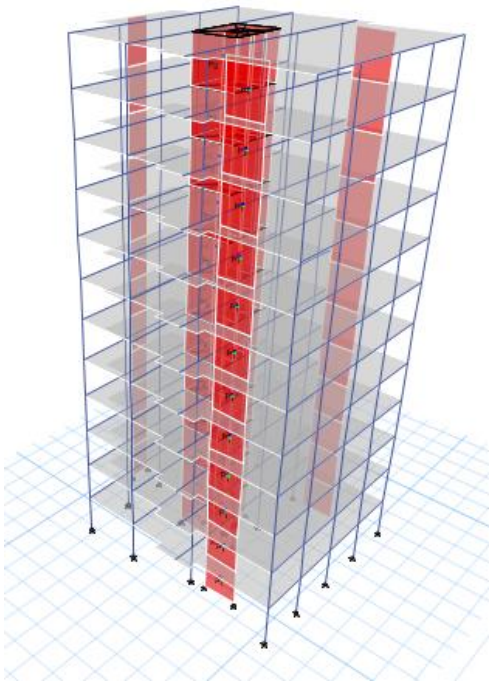

Figure IV.7. 3D view on Etabs

IV.4.3.2 Plan view

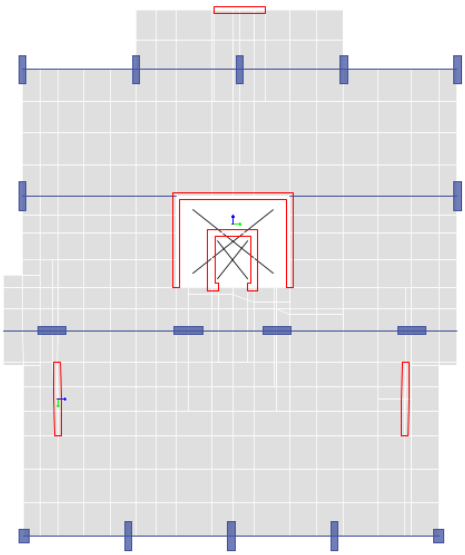

Figure IV.8. Plan view on Etabs

IV.4.3.3 Deformed shape

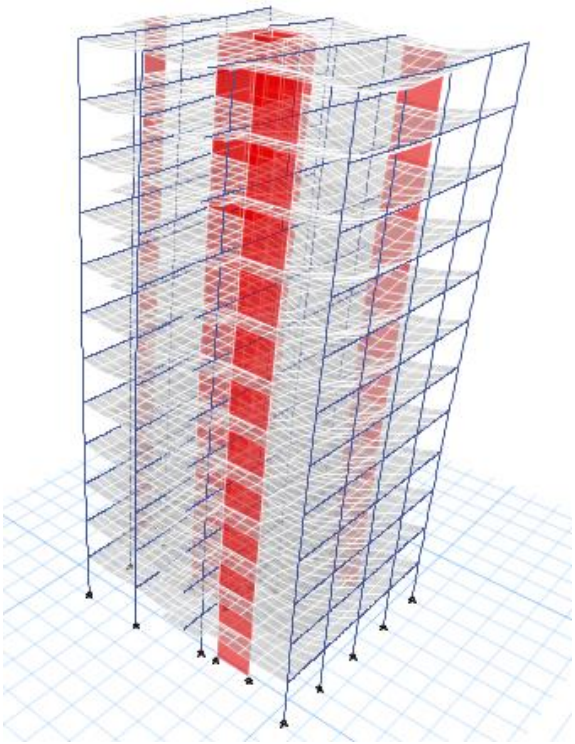

Figure IV.9. Deformed shape due to dead loads

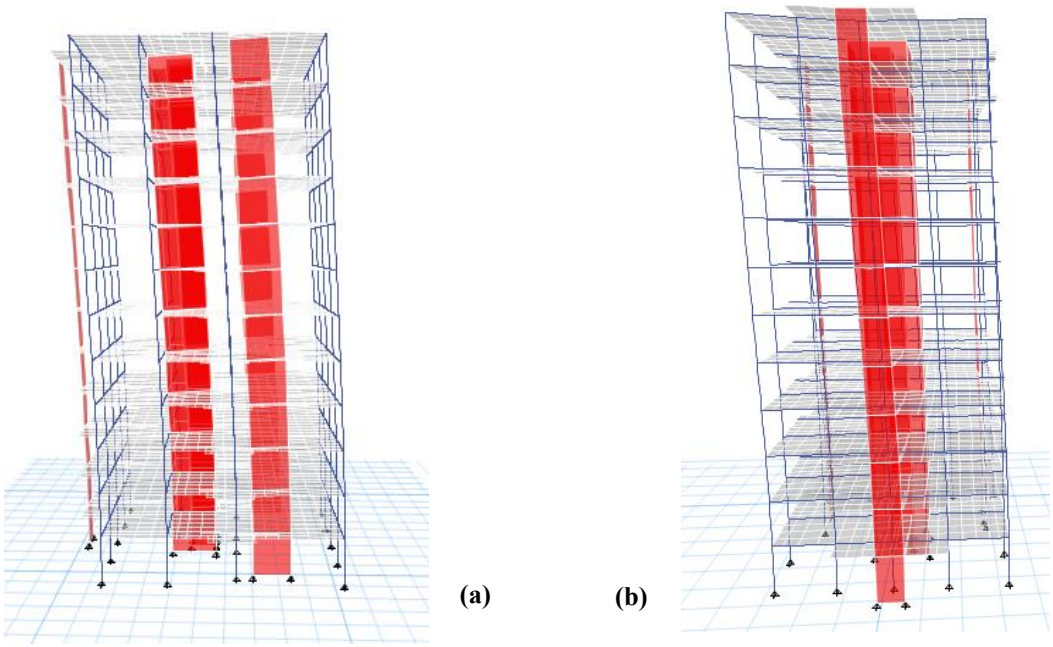

Figure IV.10. Deformed shape due to (a) EQX and (b) SpecX

IV.4.4 Structure verification

IV.4.4.1 Periods and modal participation mass ratio

Case	Mode	Period	Sum UX	Sum UY	Sum UZ	Sum RX	Sum RY	Sum RZ
		sec						
Modal	1	1.291	0.0148	0.616	0	0.307	0.0033	0.0631
Modal	2	1.196	0.1947	0.6781	0	0.3424	0.0591	0.5811
Modal	3	0.755	0.7249	0.6785	0	0.3427	0.2953	0.7496
Modal	4	0.362	0.7566	0.6792	0	0.3464	0.4356	0.8354
Modal	5	0.277	0.7569	0.8513	0	0.6423	0.4364	0.8358
Modal	6	0.192	0.8946	0.8513	0	0.6423	0.7222	0.8649
Modal	7	0.182	0.8954	0.8513	0	0.6423	0.7236	0.9157
Modal	8	0.125	0.8969	0.8513	0	0.6424	0.7285	0.9164
Modal	9	0.114	0.9029	0.8705	0	0.6833	0.7482	0.926
Modal	10	0.111	0.9067	0.9162	0	0.774	0.7593	0.9306
Modal	11	0.09	0.9449	0.9163	0	0.7741	0.8404	0.9509
Modal	12	0.078	0.9507	0.9164	0	0.7745	0.8564	0.9593
Modal	13	0.062	0.9508	0.948	0	0.8544	0.8565	0.9597
Modal	14	0.059	0.952	0.9497	0	0.8582	0.8609	0.967
Modal	15	0.057	0.97	0.9499	0	0.8587	0.9114	0.9742
Modal	16	0.055	0.97	0.9499	0	0.8587	0.9114	0.9742

Modal	17	0.048	0.9713	0.9502	0	0.8594	0.9153	0.9779
Modal	18	0.043	0.9714	0.9503	0	0.8597	0.9156	0.9781

Table IV.5. Periods and modal participation mass ratio

We notice that for the first 10 mode shapes the participating mass ratio in X and Y directions exceeds 90% so considering only the first 11 mode shapes is enough.

The building fundamental period (corresponding to mode 1) is T = 1.291 s

This building is composed of N = 11 stories, 0.1 x 11 = 1.1 and 0.3 x 11 = 3.3 s, so

$1.1 \leq T \leq 3.3$ and the period is acceptable because for an optimal seismic behavior of the structure we should have $0.1 \times N < T < 0.3 \times N$.

IV.4.4.2 Story displacement

IV.4.4.2.1 Story displacement due to wind

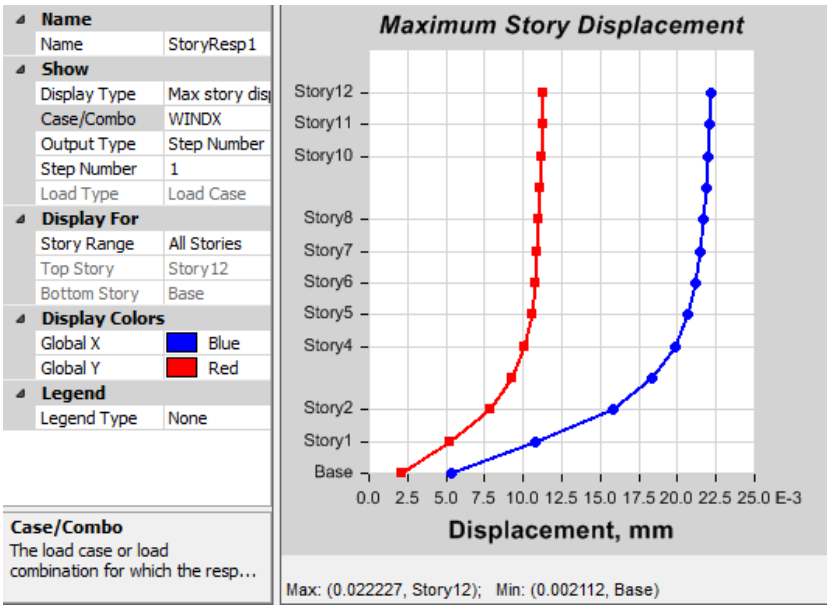

Figure IV.11. Maximum story displacement due to WindX

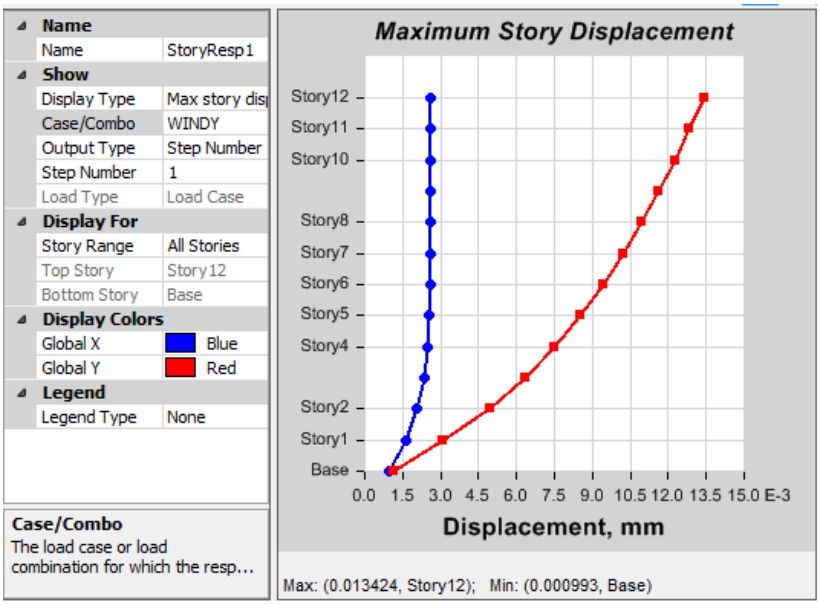

Figure IV.12. Maximum story displacement dur to WindY

The most critical displacement and drifts are due to Wind and Earthquake loads because they generate lateral forces. These lateral forces drive forward the structure to sway and to slide in x, y and z direction.

The lateral displacement of each diaphragm should not exceed:

H/500=36/500=0.072 m (H is the height from the ground floor to the roof).

Max=0.022227 mm < 0.072 m → **checked.**

IV.4.4.2.2 Story displacement due to spectrum

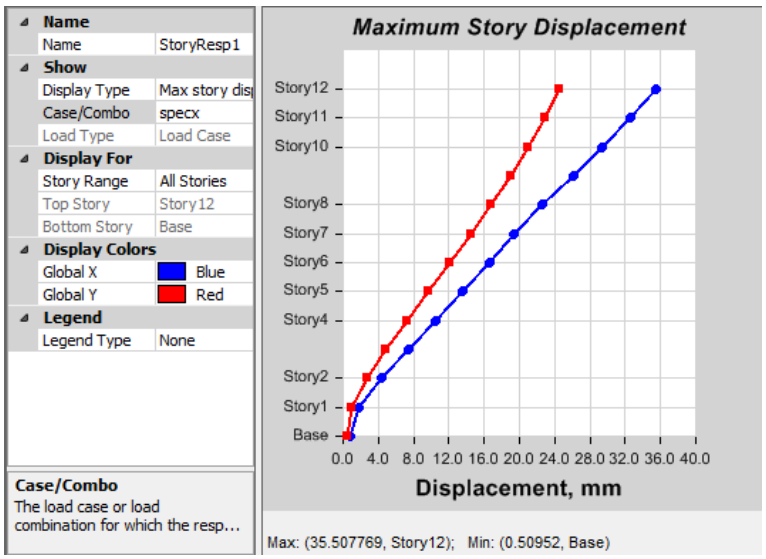

Figure IV.13. Maximum story displacement due to SpecX

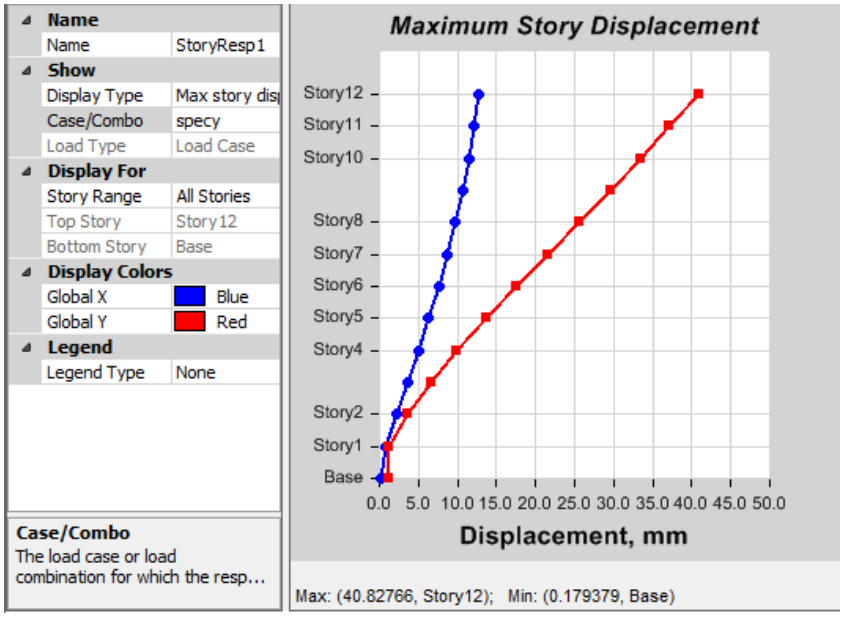

Figure IV.14. Maximum story displacement due to Specy

Max = 0.04082 mm < 0.072 m → **checked**.

IV.4.4.3 Story drift

The lateral drift between stories at all levels should be ≤ 0.02. Static Displacement = 0.7 x R x Drift = 0.7 x 5.5 x Δs_x.

The plots below confirm that the structure is stable and all the values are not getting over the maximum.

IV.4.4.3.1 Story drift due to wind

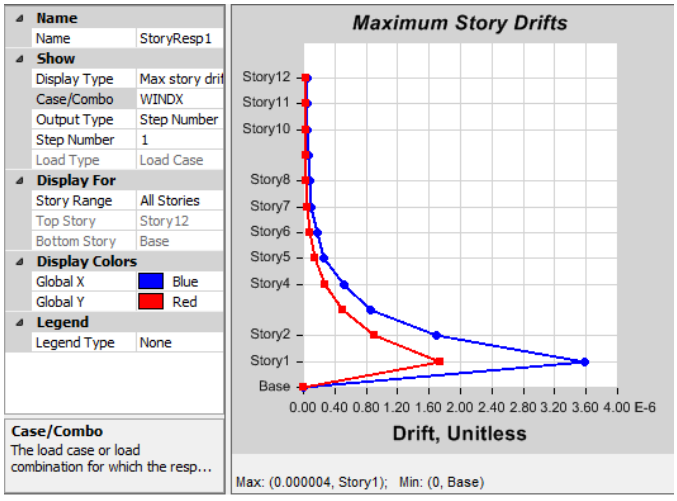

- Drift = 0.000004 < 0.02
- Static Displacement = 0.7 x R x Drift =

$0.7*8.5*\Delta s_x = 1.54e^{-05} \leq 0.02$.

Figure IV.15. Maximum story drift due to WindX

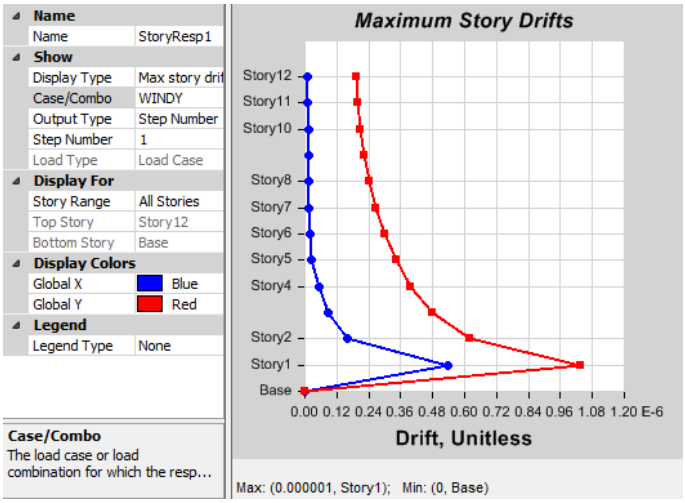

- Drift = 0.000001 < 0.02
- Static displacement= 0.7 x R x drift=

$0.7*8.5*\Delta s_x = 3.85e^{-06} \leq 0.02.$

Figure IV.16. Maximum story drift due to WindY

IV.4.4.3.2 Story drift due to spectrum

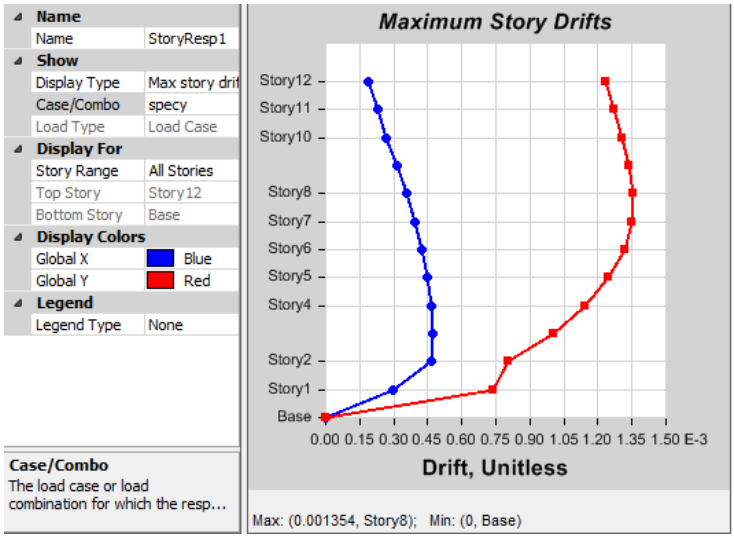

- Drift = 0.001354 < 0.02
- Static Displacement = 0.7 x R x Drift =

$0.7*8.5*\Delta s_x = 5.2e^{-3} \leq 0.02.$

Figure IV.17. Maximum story drift due to SpecX

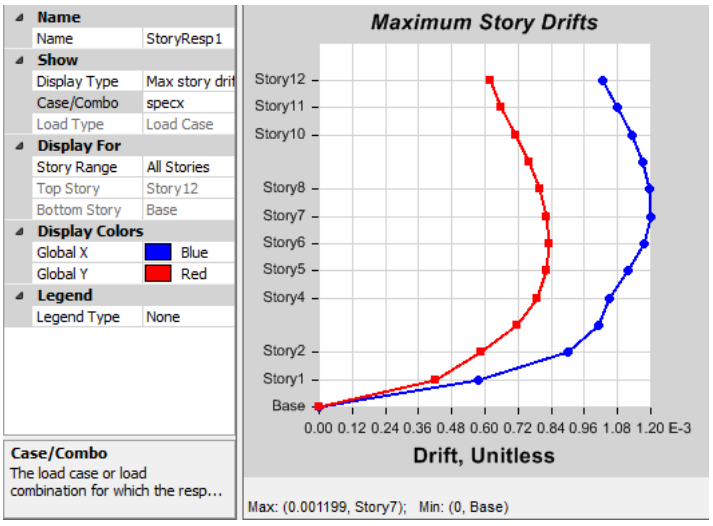

- Drift = 0.001199 < 0.02
- Static Displacement = 0.7 x R x Drift =

$0.7*8.5*\Delta s_x=4.6e^{-3} \leq 0.02$.

Figure IV.18. Maximum story drift due to SpecY

Story drift is checked for both wind and earthquake.

The drift is under the maximum allowable drift over which we should consider increasing the wall stiffness.

So we can deduce that there is no need to increase the wall dimensions in order to increase the wall stiffness.

IV.4.5 Conclusion

After checking all structural limitations and verifying that the building can support all loads that could affront them, we can proceed by designing some structural elements. The two following chapter will present the details of designing columns and shear walls.

IV.5 Column design

IV.5.1 Introduction

Columns are vertical elements of the structure that support primarily vertical loads in addition to that, columns are subjected to bending moments, shear forces and torsion. In reinforced concrete columns, compressive stress is taken by the concrete and vertical steel reinforcements. Tensile stress is taken by vertical steel reinforcements. Shear stress is taken by concrete and horizontal steel reinforcements in addition to that

horizontal ties prevent the vertical bars from premature steel buckling under compressive loads. Columns are also susceptible of buckling under compressive axial loads. It is important to classify columns in 2 categories short columns and long columns, short columns are columns which are not susceptible to buckling they normally fail by overstressing while for a long column the danger of buckling is taken into consideration and the capacity of the column is reduced.

IV.5.2 Types of columns

There are three major types of reinforced concrete columns:

- Tied columns.
- Spiral columns.
- Composite columns.

Tied columns are members having rectangular, square or circular cross section that is reinforced with longitudinal main steel to resist bending or excessive compression that might exist on the column, and its tie are placed horizontally at a spacing specified by the code.

A spiral column has a circular or square cross section, and in both cases it has continuous spiral around the longitudinal bars.

A composite column is consisted of reinforced concrete and I-Beam steel shape or a steel tube filled with concrete. In composite columns we should use a high strength concrete so that the modulus of elasticity of concrete is relatively closer to the one of the steel in order for the concrete to have the sufficient stiffness to carry a relatively good part of the vertical loads.

IV.5.3 ACI code provisions for column design

For columns, as for all members designed according to ACI Code, adequate safety margins are established by applying load factors to the service loads and strength reduction factors to the nominal strengths. Thus, for columns $\boldsymbol{Pn} \geq \boldsymbol{Pu}$ and $\boldsymbol{Mn} \geq \boldsymbol{Mu}$ are the basic safety criteria. For most members subjected to axial compression or compression plus flexure (compression controlled members), the ACI Code provides basic reduction factors φ:

- 0.65 for tied columns.
- 0.7 for spirally reinforced columns.

IV.5.4 Hints for design according to the ACI building requirement code

IV.5.4.1 Cover

There are two cases to take into consideration:

- If the concrete element is exposed to weather: cover c ≥ 50 mm
- If the concrete element is not exposed to weather: cover c ≥ 40 mm

IV.5.4.2 Main reinforcements

- **Vertical reinforcements**

The vertical steel ratio ρt is formulated as:

$$\rho t = \frac{Ast}{Ag} \qquad \text{(IV.1)}$$

Where

Ast: is the total area of vertical bars

Ag: is the gross section area of concrete section

Boundaries of steel ratio ρt:

- ρt_{min} = 1 %
- ρt_{max} = 8 %

Minimum number of bars:

- The minimum number of vertical bars in a rectangular or square tied column is 4
- The minimum number of vertical bars in a circular tied column is 6
- The minimum number of vertical bars in spiral column is 6

Spacing:

The spacing S between vertical reinforcements should be Smin ≤ S ≤ Smax
Smin ≥ min {1.4 db; 40 mm}
Smax ≤ 150 mm

Where db is the diameter of the vertical bar

- **Lateral reinforcements**

For tied columns:

dt ≥ db/3
Stmin ≤ St ≤ Stmax
Stmax ≤ min {16 db; 48 dt; b (smallest dimension of the column)}
Stmin ≥ 40 mm

For spiral columns:

The ratio of spiral reinforcements ρs is:

$$\rho s \geq 0.45\left(\frac{Ag}{Ac}-1\right)\frac{f'c}{fy} \quad \text{(IV.2)}$$

$$Asp = \frac{\rho s \times dc \times st}{4} \quad \text{(IV.3)}$$

Where

Ag: is gross section area concrete cross section

Ac: is the area of the concrete confined in the spiral

Asp: is the area of the spiral bar

Dc: is the diameter of the spiral

St: is the pitch of the spiral

Stmin ≤ St ≤ Stmax

Stmin ≥ 25 mm

Stmax ≤ 80 mm

IV.5.5 Design of columns

The design of the columns is made based on the **ACI 318-05**. The softwares used are ETABS and S-CONCRETE.

IV.5.5.1 Loads from Etabs

The following figure shows the column C13 that will be designed and detailed.

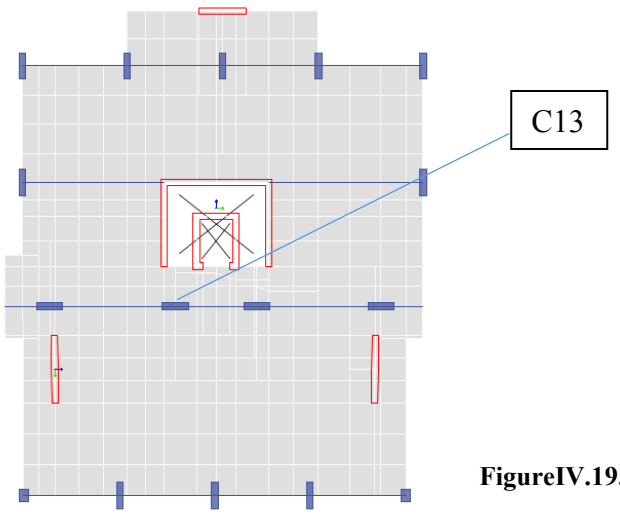

FigureIV.19. Chosen column for design

The loads are obtained from the plastic file (using the ultimate combinations) and then they are copied to the S-concrete.

IV.5.5.2 Design of columns using S-CONCRETE

S-CONCRETE is a software that provides a more detailed design of the structural elements (regular beams, columns and walls). After entering the shape of the section, its dimensions, concrete and steel characteristics, the building code to use, the slenderness effect data and the dimension of bars to use. Then the internal solicitations in the structural element (column in our case) are imported from Etabs to S-Concrete and then the software displays the demand over capacity ratio for axial stresses and for shear stresses. It is now up to the designer to choose the appropriate reinforcements.

- Column C13 at all levels

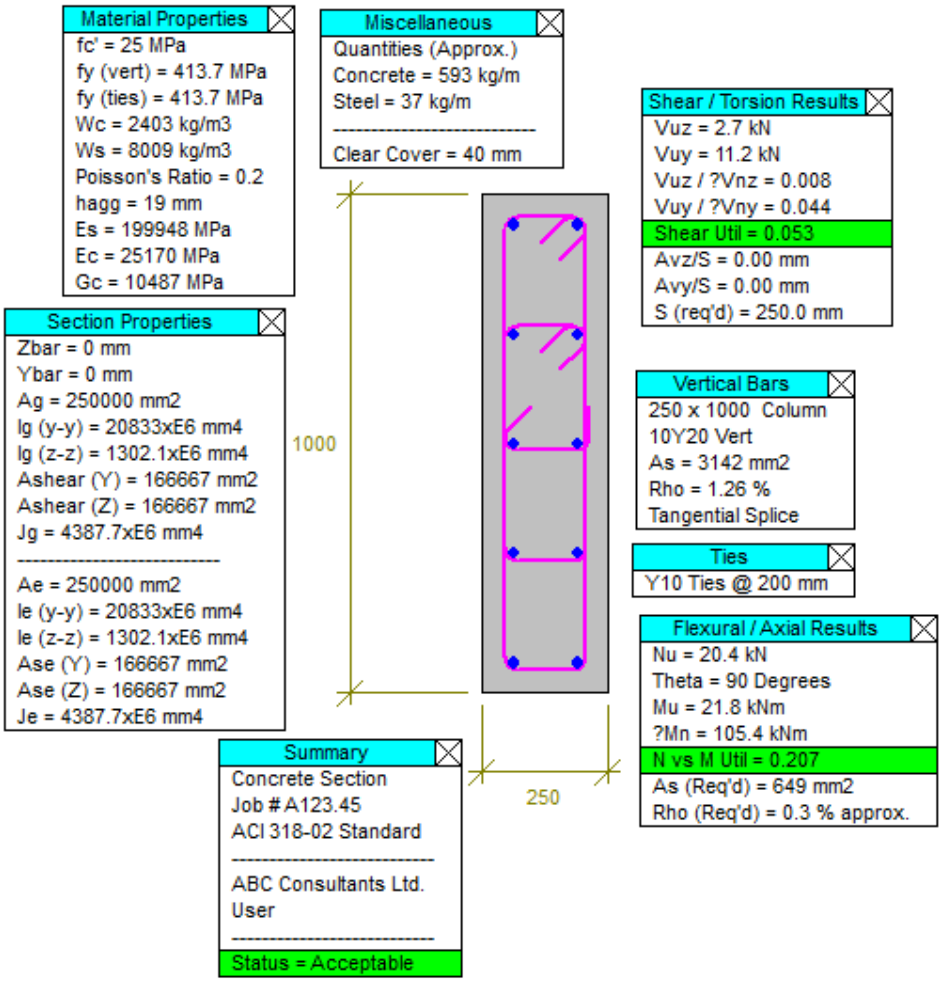

Figure IV.20. Steel reinforcement of column C13 provided by S-concrete at story 1

- Longitudinal section of column C13:

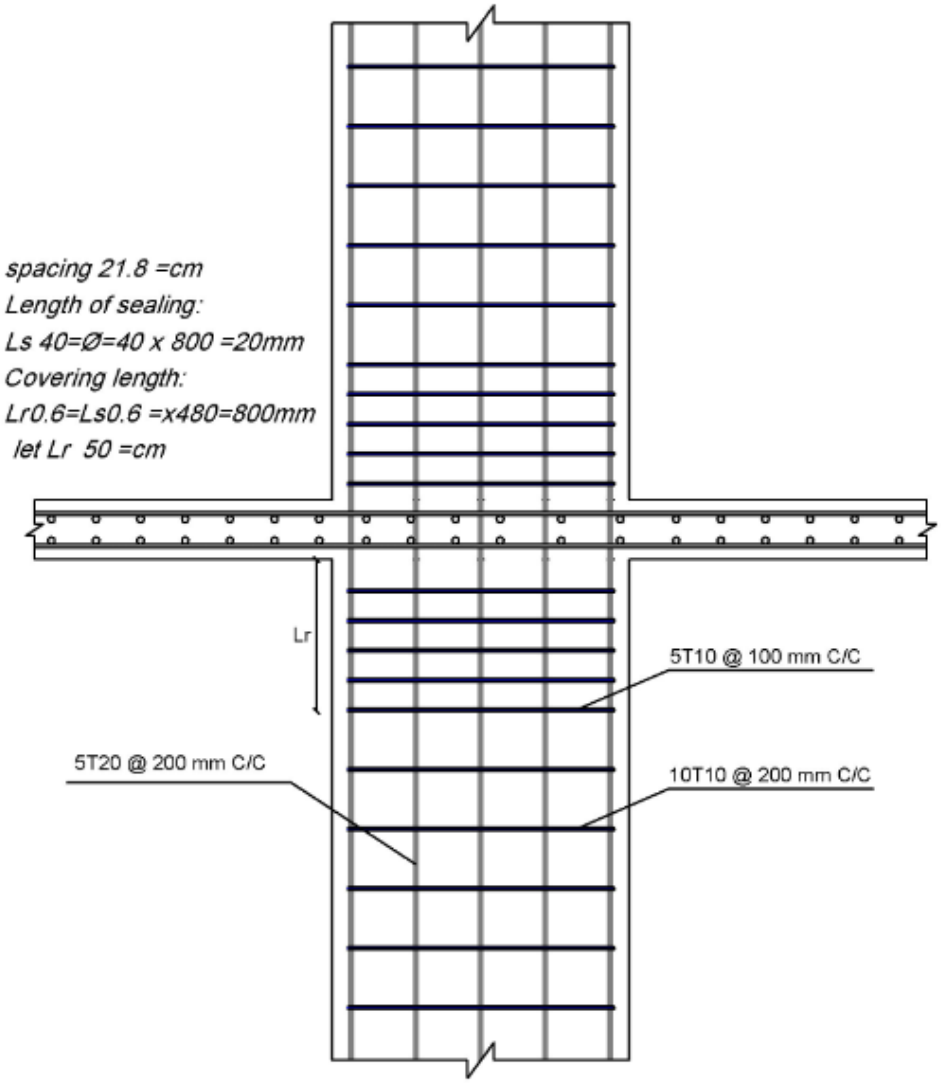

Figure IV.21. Longitudinal cut section of column C13

IV.6 Shear wall design

IV.6.1 Introduction

In structural engineering, a shear wall is a wall composed of braced panels (shear panels) to counter the effects of lateral load acting on a structure. Wind and earthquake loads are the most common loads that shear walls are designed to counteract.
A shear wall is a wall designed to resist the shear due to lateral loads. Many building codes mandate the use of shear walls to make homes safer and more stable, and learning about shear walls is an important part of an architectural education. Architects are obliged to think about shear walls and other safety features when they design a structure, so that they can accommodate the walls to make the structure safe while also esthetically pleasing.

IV.6.2 Analysis criteria in Etabs

On ETABS, we assign the walls as piers. Then, we export all the loads solicitations in the piers to S-Concrete to obtain the final design and drawing.
ETABS software allows the determination of the internal forces in these elements with:

- The conventional finite elements shell results: Normal and shear stresses, Normal and shear forces, Out-of-Plane moments.
- The Pier results of wall: an assembly of walls (core), giving the resulting forces at the center of gravity of the wall sections, in the same manner of column results: Normal Forces, Shear Forces, Flexural and Torsion Moments. The wall pier element internal forces are similar to the frame element internal forces. They are:

    - P the axial force.
    - V_2 the shear force in direction 2.
    - V_3 the shear force in direction 3.
    - T the axial torque.
    - M_2 the bending moment carried by the axis 2.
    - M_3 the bending moment carried by the axis 3.

The following figure shows the shear wall studied in this project:

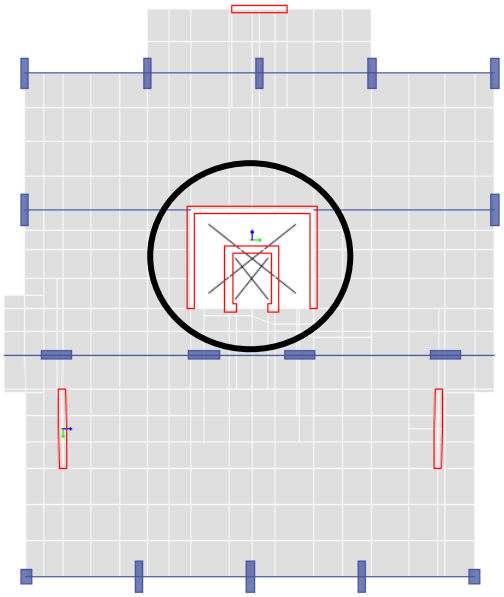

Figure IV.22. Chosen shear wall for design

IV.6.3 Design of the shear wall

The design of shear walls is made on S-CONCRETE.

The U-shear wall studied has a regular shape, so all what is needed is to copy the ultimate loads obtained in Etabs to the S-CONCRETE and do the design. Designing a wall on this software is similar to the way we designed columns.

The following figure shows the design of the wall at story 1:

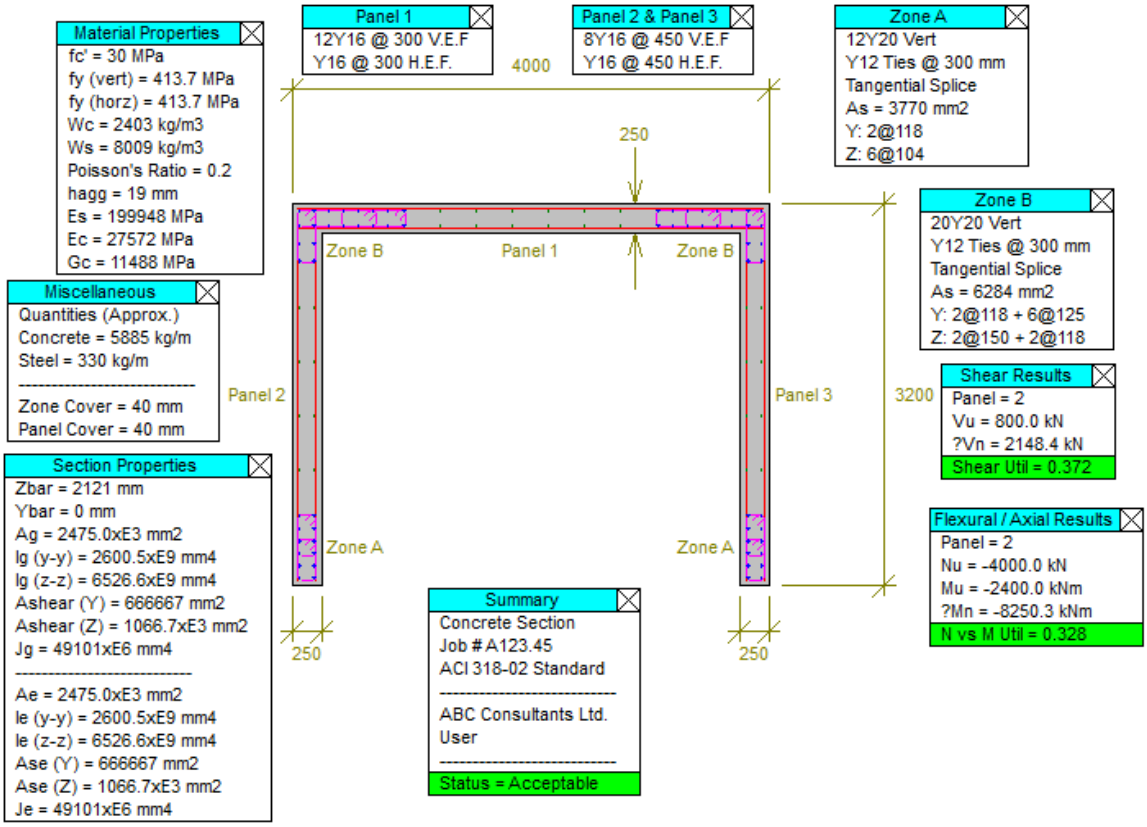

Figure IV.23. Reinforcement of shear wall provided by S-concrete at story 1

IV.7 Slab design

IV.7.1 Introduction

Selecting the most effective floor system can be vital to achieving overall economy, especially for low- and mid-rise buildings and for buildings subjected to relatively low lateral forces where the cost of the lateral-force-resisting system is minimal. Concrete, reinforcement, and formwork are the three primary expenses in cast-in-place concrete floor construction to consider throughout the design process, but especially during the initial planning stages.

IV.7.2 Preliminary sizing of the slab.

Before analyzing the floor system, one must assume preliminary member sizes. Typically, the slab thickness is determined first to ensure that the deflection requirements of ACI 318-05, Section 9.5 are satisfied.

In this project, the thickness of the slab is considered to be 20 cm. This thickness will be checked later to ensure that the deflection requirements are satisfied.

IV.7.3 Design on SAFE

SAFE is the ultimate tool for designing concrete floor and foundation systems. From framing layout all the way through to detail drawing production, SAFE integrates every aspect of the engineering design process in one easy and intuitive environment.

Laying out models is quick and efficient with the sophisticated drawing tools, or use one of the import options to bring in data from CAD, spreadsheet, or database programs. Slabs or foundations can be of any shape, and can include edges shaped with circular and spline curves.

Mats and foundations can include nonlinear uplift from the soil springs, and a nonlinear cracked analysis is available for slabs. Generating pattern surface loads is easily done by SAFE with an automated option. Design strips can be generated by SAFE or drawn in a completely arbitrary manner by the user, with complete control provided for locating and sizing the calculated reinforcement. Finite element design without strips is also available and useful for slabs with complex geometries.

The following figure shows the slab model on SAFE

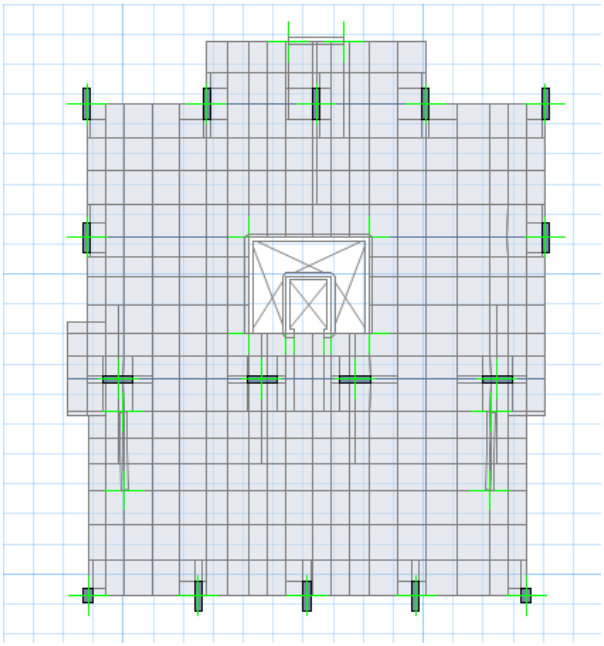

Figure IV.24. Floor plan mesh on SAFE

IV.7.4 Maximum allowable Deflection:

The largest clear span in the story is L_n = 6 m.

The maximum allowable deflection is $\frac{L_n}{240} = \frac{6000}{240} = 25\ mm$

IV.7.5 Loads:

IV.7.5.1 Dead Load:

Dead load = Self weight of the slab + Super Imposed Dead Load (SIDL)

- S.W. of slab: 0.2*25=5 KN/m^2
- SIDL = 3 KN/m^2

So D.L. =8 KN/m^2= 0.8 ton/m^2

IV.7.5.2 Live Load:

L.L. =3.5 KN/m^2=0.35 ton/m^2

IV.7.5.3 Uniformly Distributed Load:

Service Load = W_S = DL + LL = 0.8+ 0.35 = 1.15 ton/m^2.

Ultimate Load = W_u = 1.2DL + 1.6LL = 1.2*0.8+1.6*0.35 = 1.52 ton/m^2 (According to ACI 318-11).

IV.7.6 Results on SAFE

IV.7.6.1 Deformed shape under service load

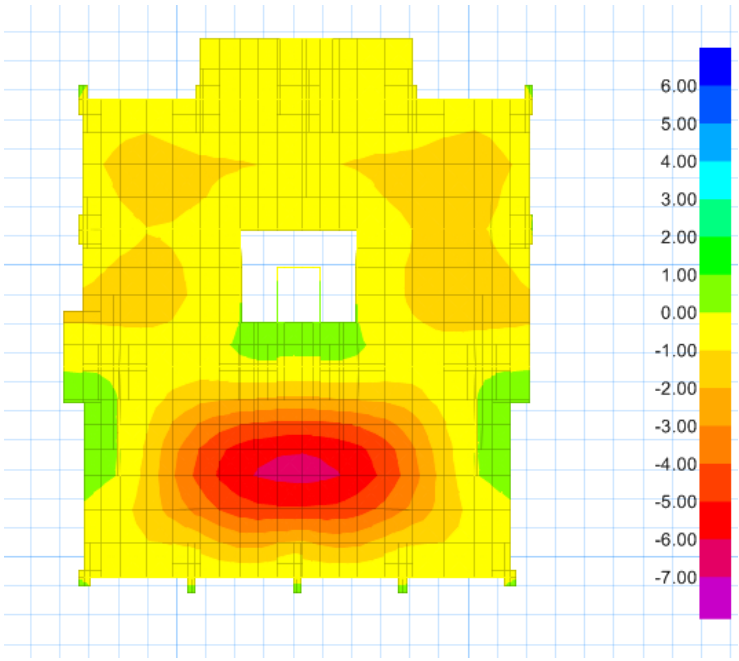

Figure IV.25. Deformed shape under service loads

The maximum deflection is 6.36 mm < 25 mm, then checked.

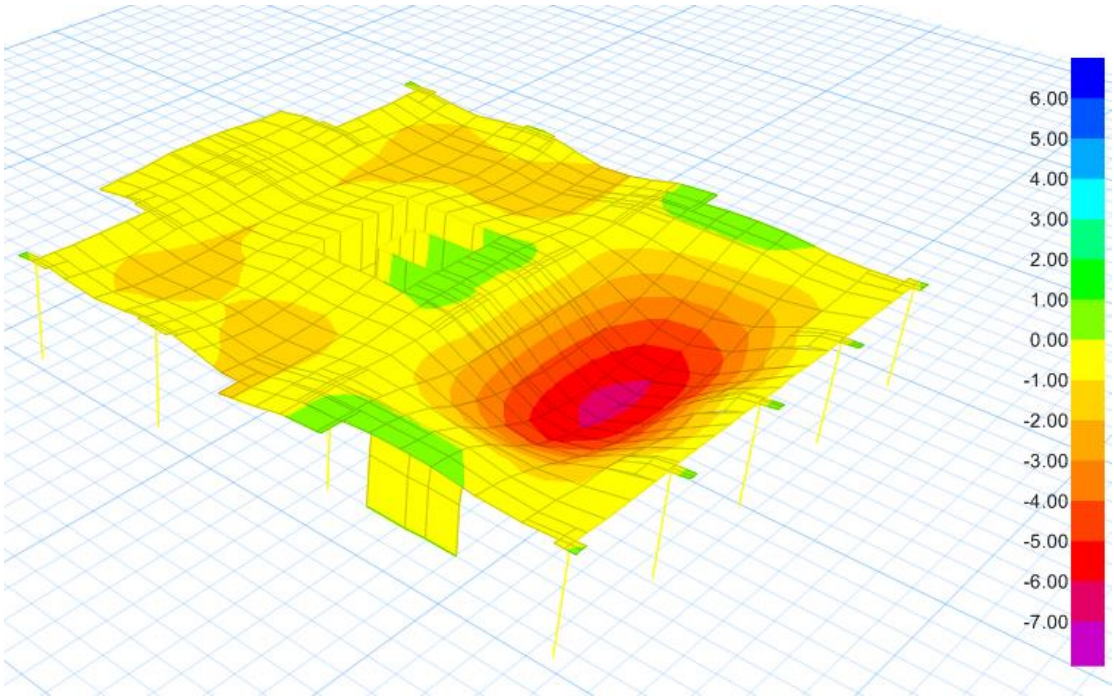

Figure IV.26. 3D view of the deformed shape

IV.7.6.2 Reinforcement of the slab

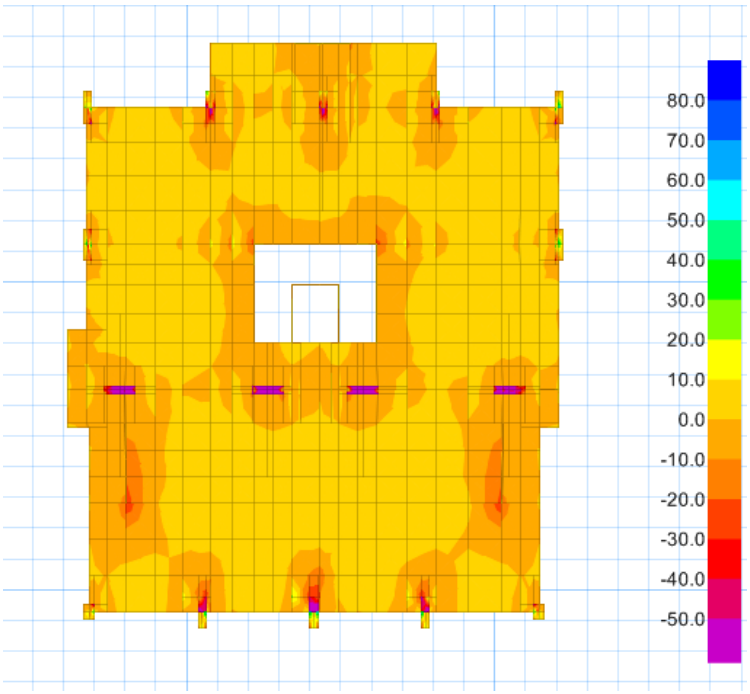

Figure IV.27. Mxx (KN.m/m) under ultimate combination

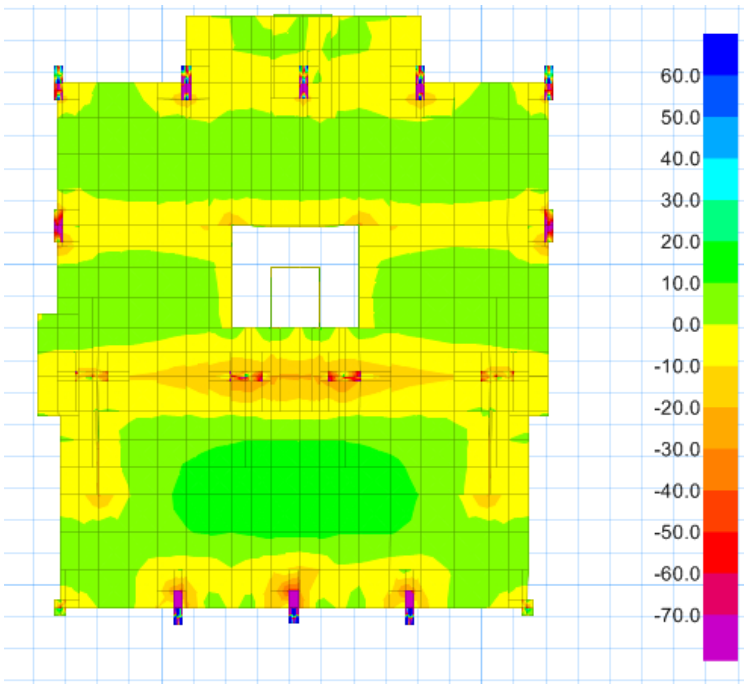

Figure IV.28. Myy (KN.m/m) under ultimate combination

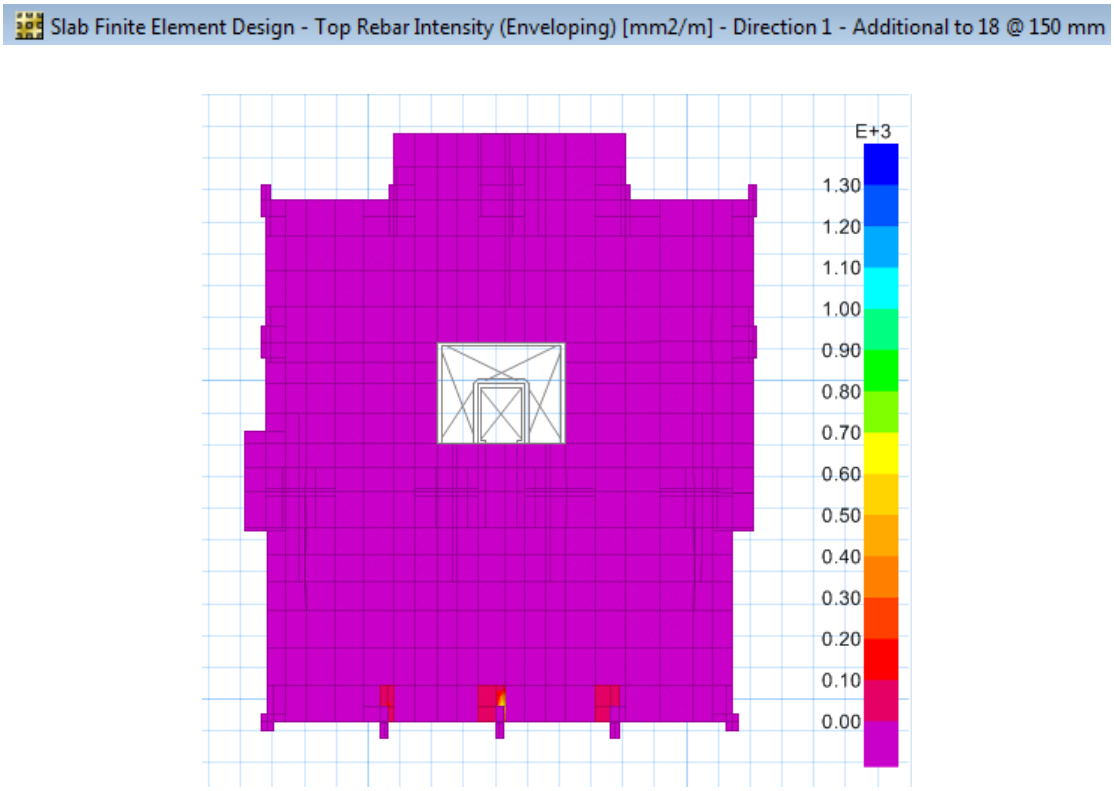

Figure IV.29. Top rebar Intensity-Direction 1

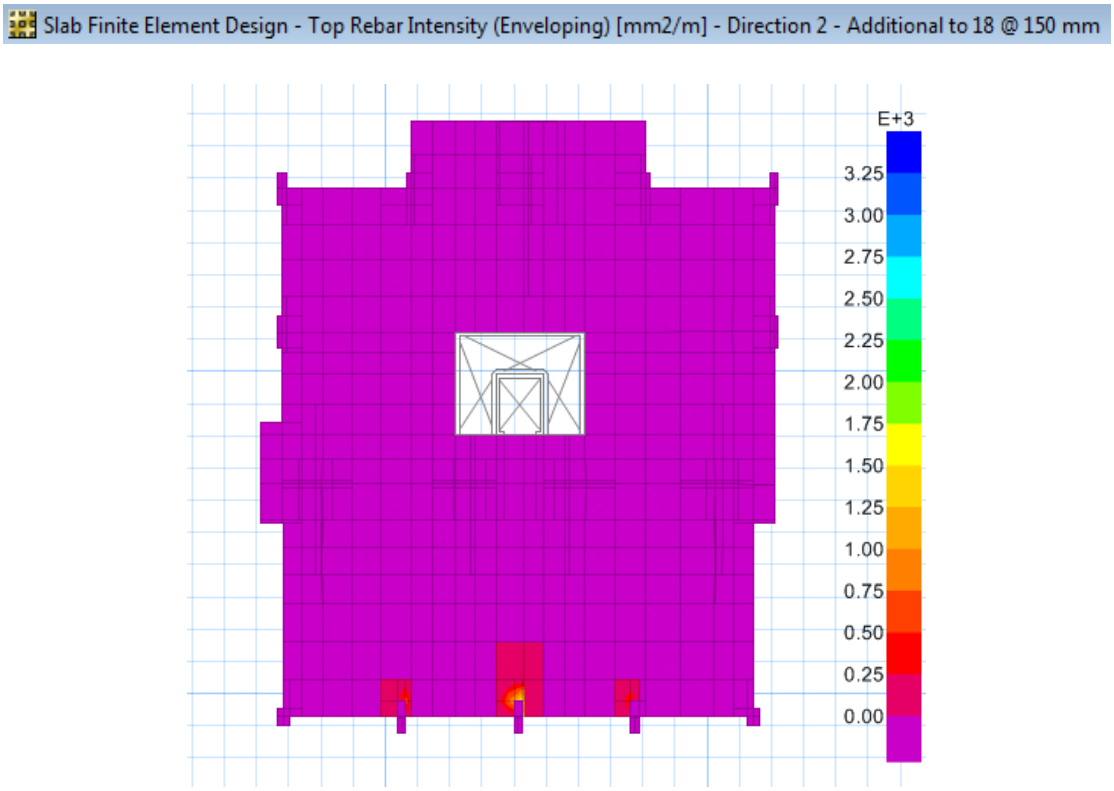

Figure IV.30. Top rebar Intensity-Direction 2

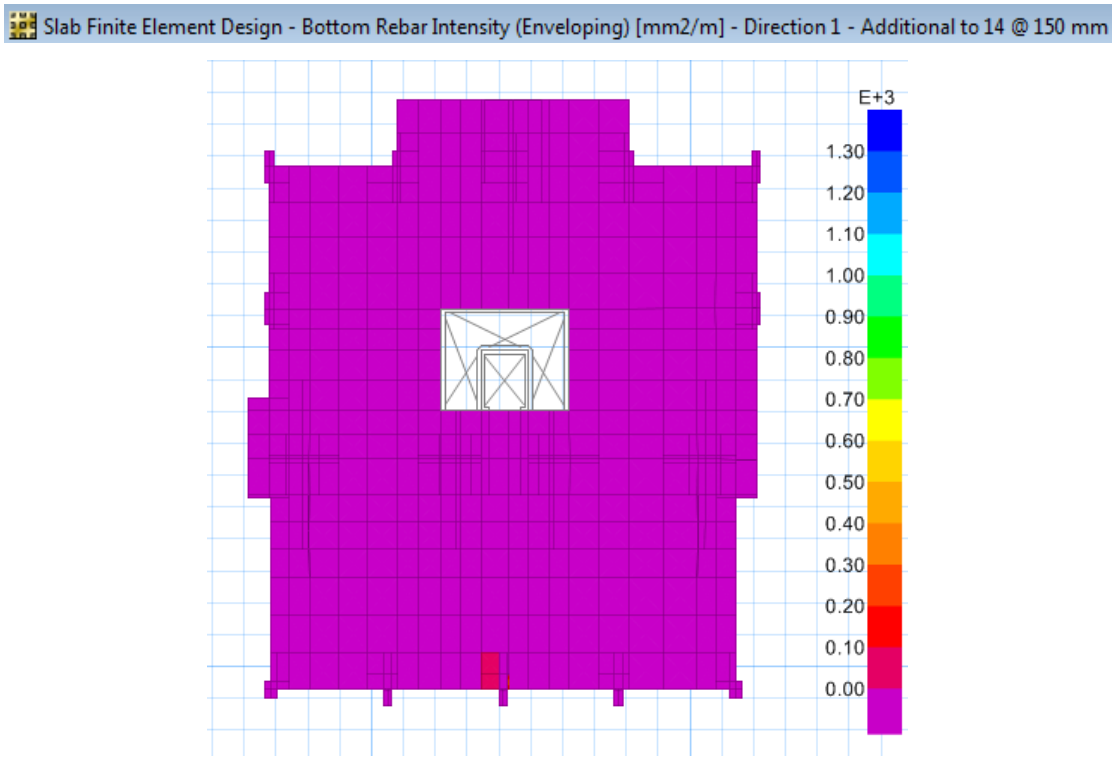

Figure IV.31. Bottom rebar Intensity-Direction

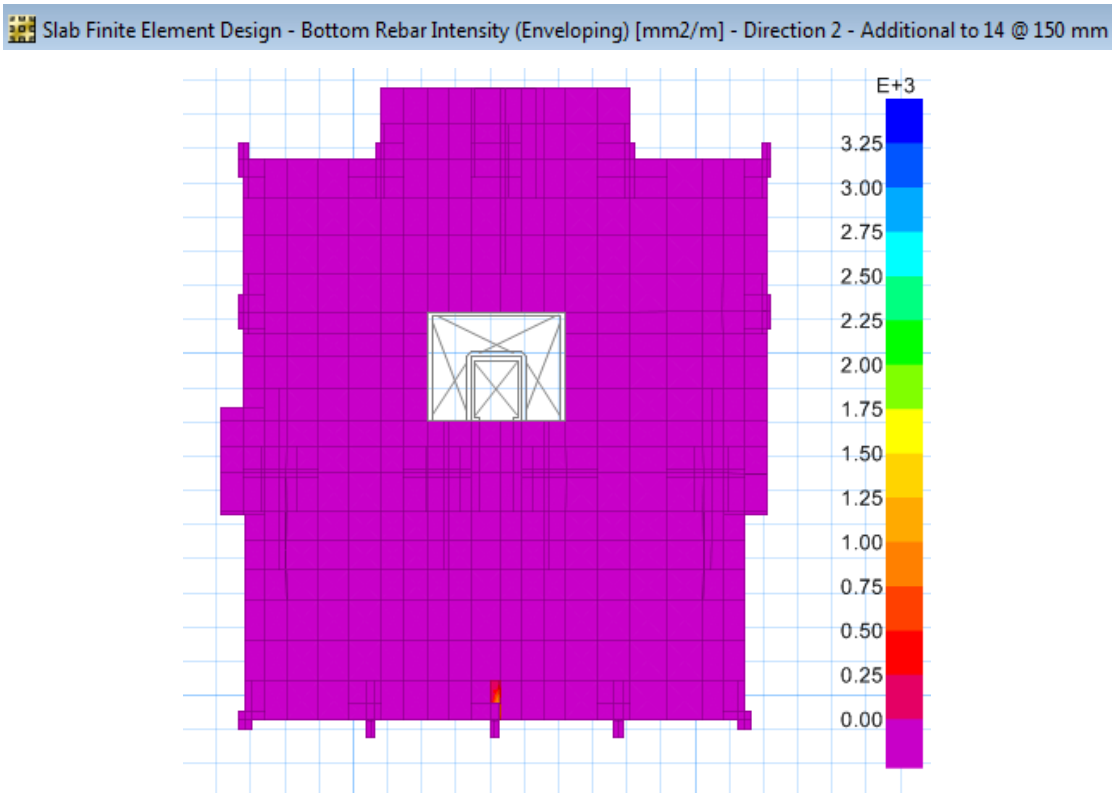

Figure IV.32. Bottom rebar Intensity-Direction 2

IV.7.6.3 Top reinforcement

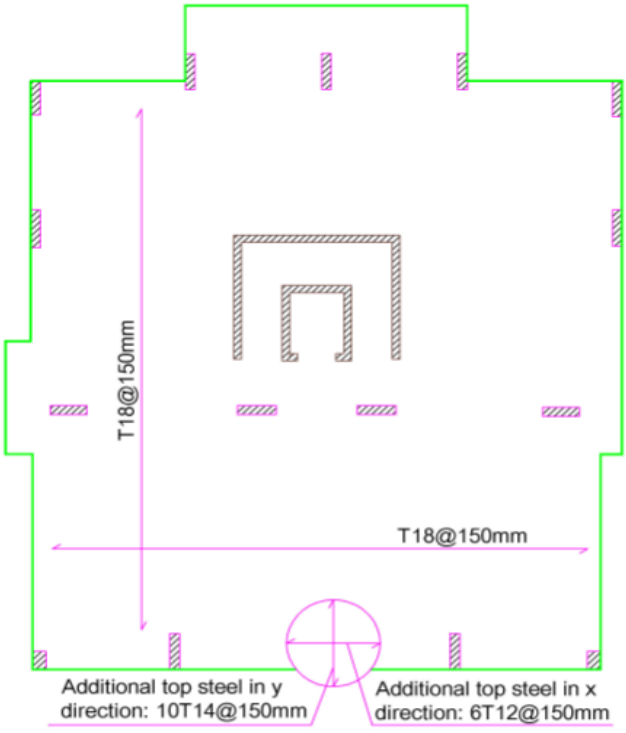

Figure IV.33. Top reinforcement

IV.7.6.4 Bottom reinforcement

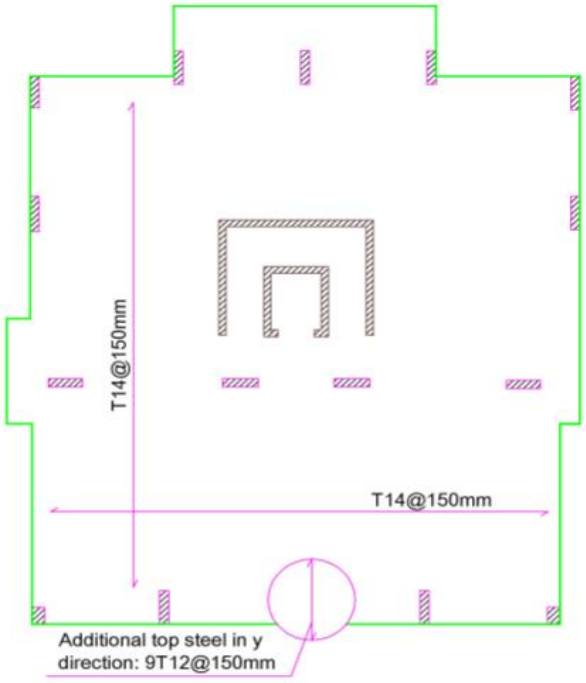

Figure IV.34. Bottom reinforcement

IV.8 Raft foundation design

A mat foundation is a large concrete slab used to interface one column, or more than one column in several lines, with the base soil.

IV.8.1 Design of mat foundation

There are several methods to design a mat (or plate) foundation:

1) An approximate method. The mat is divided into strips loaded by a line of columns and resisted by soil pressure. This strip is then analyzed as a combined footing. This method can be used where the mat is very rigid and the column pattern is fairly uniform in both spacing and loads. This method is not recommended at present because of the substantial amount of approximations and the wide availability of computer programs that are relatively easy to use—the finite grid method. A mat is generally too expensive and important not to use the most refined analytical methods available.
2) Approximate flexible method. This method was suggested by ACI Committee 336 (1988) and is briefly described here, and the essential design aids are provided. If this method is used it should be programmed as for the AIRPAVE computer program noted in subsection 10-6.2 following.
3) Discrete element methods. In these the mat is divided into elements by gridding. These methods include the following:
   a. Finite-difference method (FDM)
   b. Finite-element method (FEM)
   c. Finite-grid method (FGM)

IV.8.2 Modeling process

We are going to design our mat foundation using “SAFE” software.

The subgrade modulus of the soil K_s is also defined and this soil is assigned to the mat.

The loads are exported from ETABS and so the combinations.

We must also assign new LL and new SIDL to the mat drawn on SAFE.

Generally we take: SIDL =2.5kN/m^2

LL = 3 kN/m^2

After calculation, the mat is divided into a number of discrete points (finite elements), so we can get all the necessary results such moment, steel, settlement, soil reaction…

1- Define soil support with a bearing capacity

Soil type: Sc → Very dense soil and soft rock.

Bearing capacity: q =12tons/ft^2 ≈ 1150 kN/m^2 = 1150 kPa.

Allowable bearing capacity: q_a= q/3 = 350 kPa.

We consider the thickness of the raft to be about 1.2m, this thickness will be later verified and checked and f'$_c$ is chosen to be equal to 30 MPa.

IV.8.3 Safe model

IV.8.3.1 Deformed shape

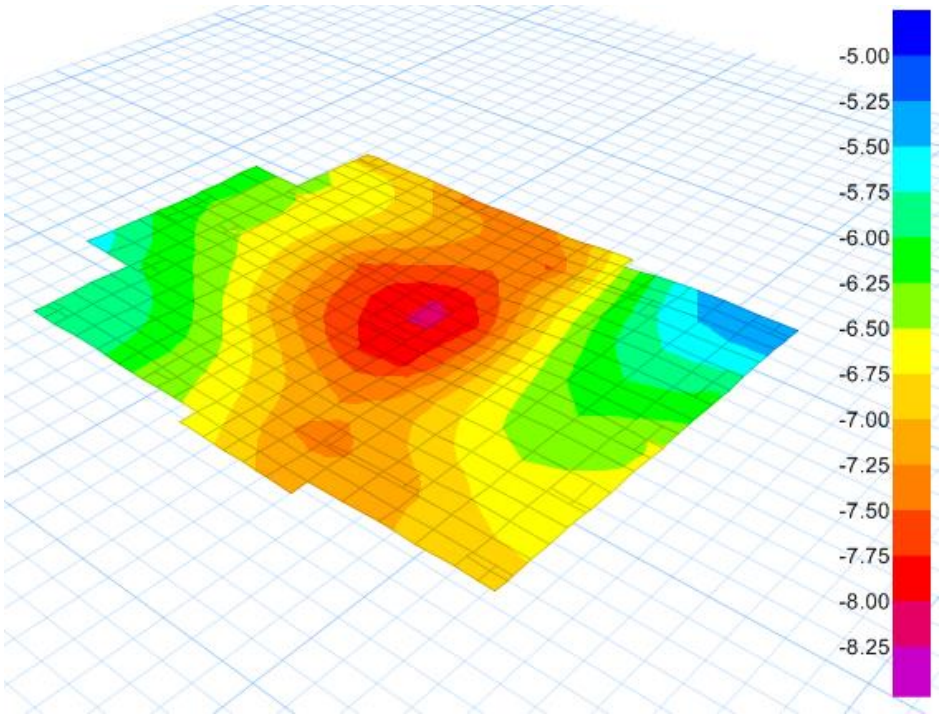

Figure IV.35. Deformed shape under service loads

The maximum settlement is equal to 8.03 mm which is smaller than 50 mm, so checked.

IV.8.3.2 Soil pressure

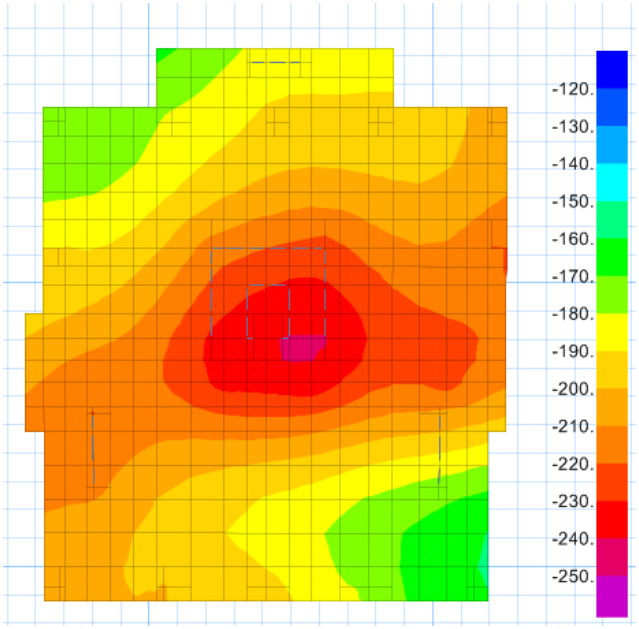

Figure IV.36. Soil pressure under the raft foundation due to service load

The highest soil pressure under raft (service combination) is 240.94 KN/m^2 which is lower than the allowable bearing capacity q_a = 350 KN/m^2 → the soil can support the load applied to it and no need for piles.

IV.8.3.3 Punching shear ratios

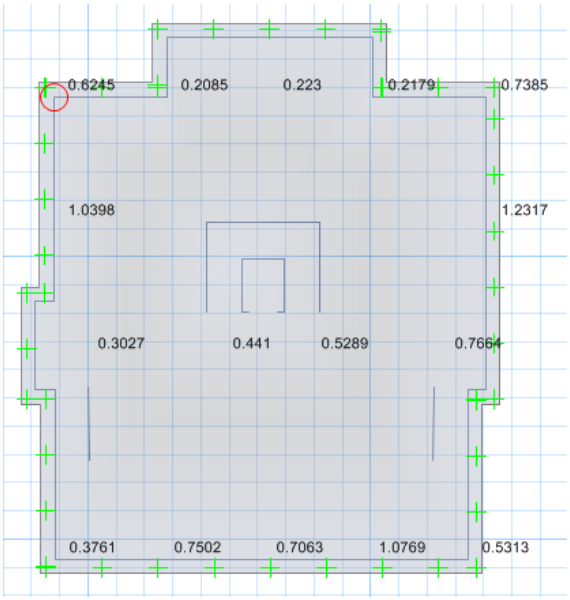

Figure IV.37. Punching shear ratios with 1.2m thickness

As we can see, there are 3 punching shear ratios greater than 1, so we need to increase the thickness of the raft. Let it be 1.35m.

After increasing the thickness to 1.35m, we can see that all verifications are checked and almost all the punching shear ratios are smaller than 1, so we can deduce that the thickness 1.35 m is acceptable.

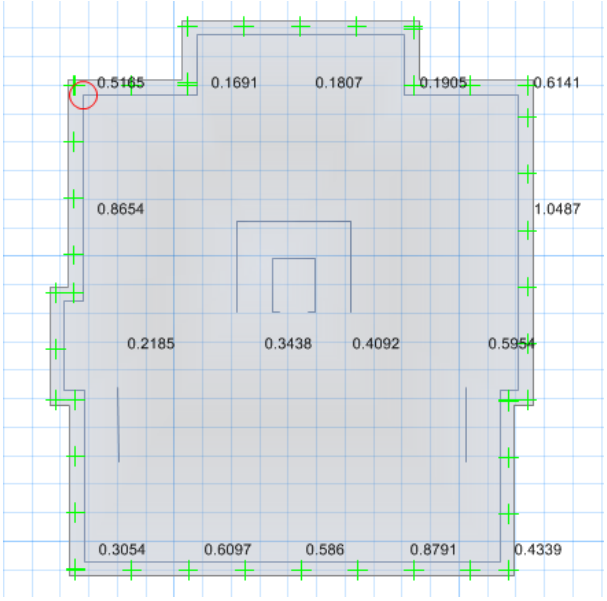

Figure IV.38. Punching shear ratios with 1.35m thickness

IV.8.4 Moments

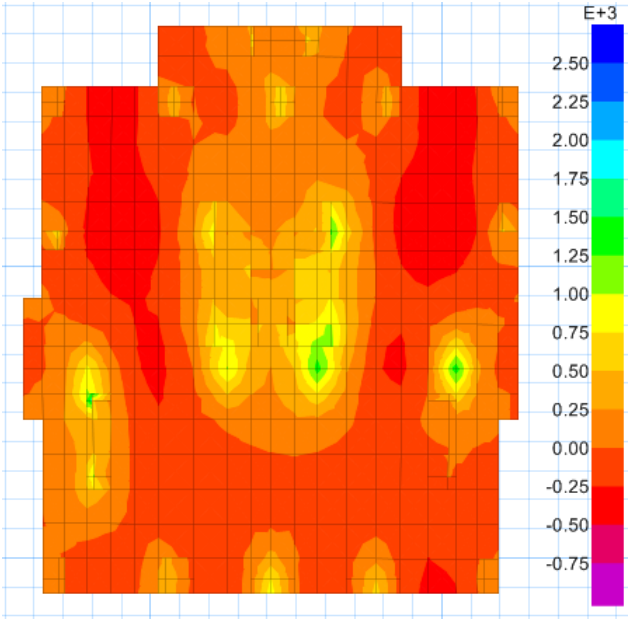

Figure IV.39. Mxx (KN.m/m) under ultimate combination

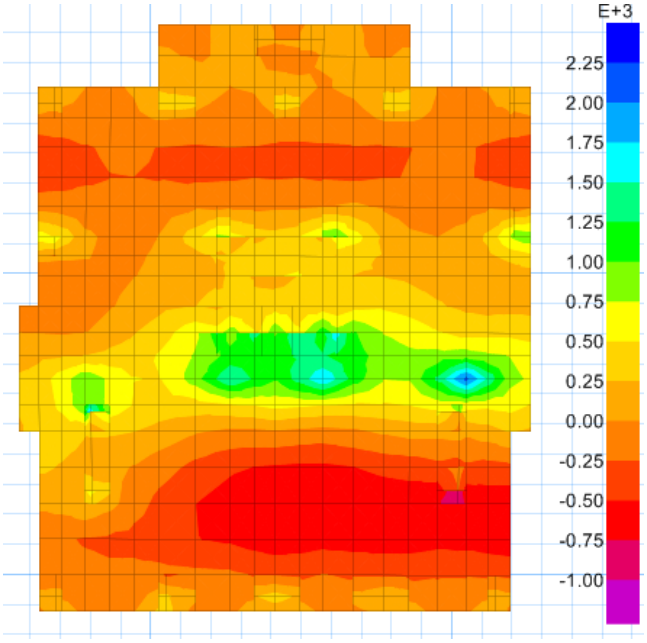

Figure IV.40. Myy (KN.m/m) under ultimate combination

IV.8.5 Reinforcement of the raft

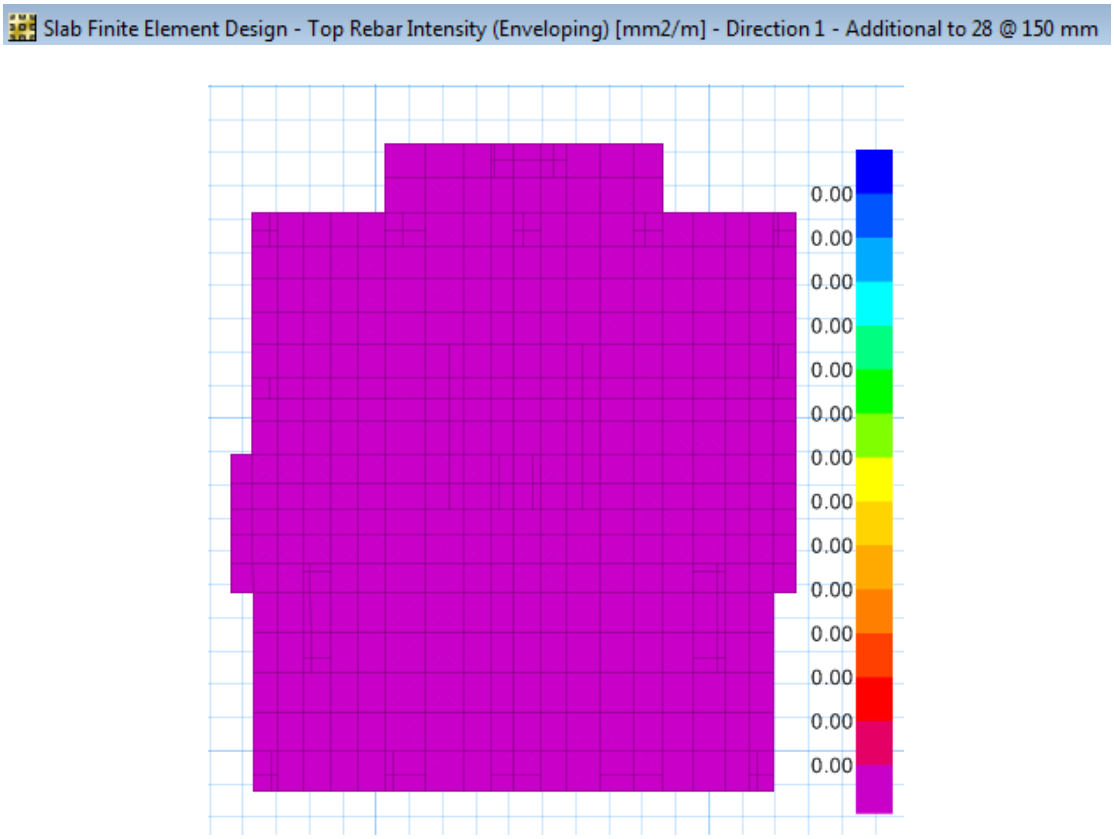

Figure IV.41. Top rebar intensity-direction 1 & 2

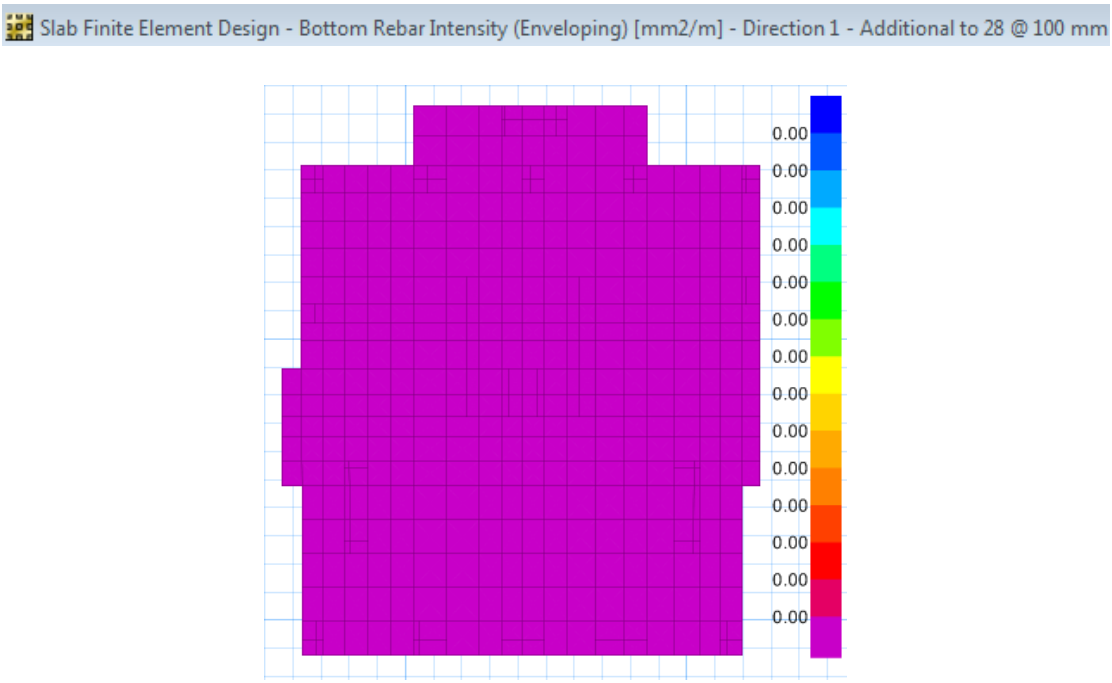

Figure IV.42. Bottom rebar intensity-direction 1 & 2

IV.8.6 Reinforcement details

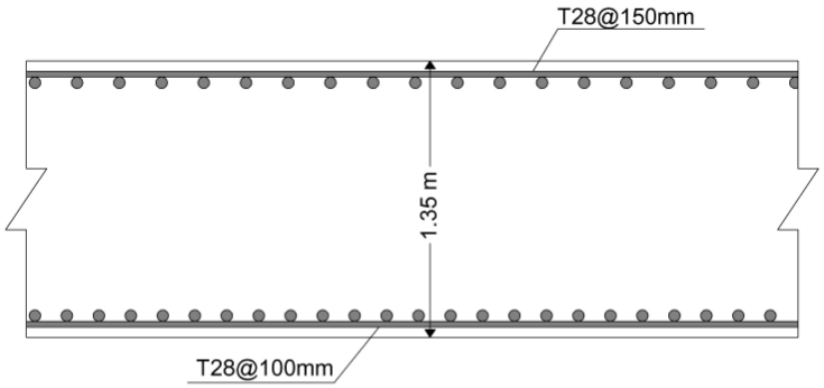

Figure IV.43. Reinforcement detail for raft foundation

General Conclusion

This study focuses on the probabilistic analysis of shallow foundations resting on spatially varying soils. One aleatory source of uncertainty was considered. It is the soil (or rock) spatial variability which was modeled by random fields.

In this project, a literature review on the soil and the meta-modeling techniques was first presented. It was followed by two main parts.

The first part (which is composed of chapters II, III) presents a probabilistic analysis of shallow foundations resting on spatially varying soils or rocks and subjected to a static loading. Both cases of square and rectangular footings were studied. In this part, the probabilistic method used to calculate the different probabilistic outputs was the Sparse Polynomial Chaos Expansion (SPCE) methodology and its extension the SPCE/GSA procedure.

In chapter II and III, the effect of the spatial variability in three dimensions (3D) was investigated through the study of the ultimate bearing capacity of square and rectangular foundations resting on a purely cohesive soil with a spatially varying cohesion in the three dimensions. This case involves relatively non-expensive deterministic models although a 3D mechanical model was used. This is because of the use of a purely cohesive soil.

The main findings of the first part can be summarized as follows:

- Chapters II and III have shown the superiority of the SPCE with respect to the classical MCS commonly used in geotechnical engineering problems involving spatially varying soils.
- The decrease in the autocorrelation distances (a_h or a_v), lead to a less spread out PDF of the system response.
- When a small number of variables is used, the SPCE/GSA methodology is hard to be executed.
- The probabilistic ultimate bearing capacity coefficient N_c increases with increasing variation of the autocorrelation distance.

The second part (which corresponds to chapter IV) was about designing the main structural elements of a residential building. The design was made using many softwares. The study of this building has led to make the reinforcement of the basic elements: column, shear wall, slab and raft design.

References

1. T. Al-Bittar and A.-H. Soubra (2014), "Efficient sparse polynomial chaos expansion methodology for the probabilistic analysis of computationally-expensive deterministic models". *INTERNATIONAL JOURNAL FOR NUMERICAL AND ANALYTICAL METHODS IN GEOMECHANICS, Volume 38, Issue 12, Pages: 1211–1230.*

2. T. Al-Bittar and A.-H. Soubra (2013), "Bearing capacity of strip footings on spatially random soils using sparse polynomial chaos expansion". *INTERNATIONAL JOURNAL FOR NUMERICAL AND ANALYTICAL METHODS IN GEOMECHANICS, Volume 37, Issue 13, Pages: 2039–2060.*

3. T. Al-Bittar and A.-H. Soubra (2014), "Probabilistic Analysis of Strip Footings Resting on Spatially Varying Soils and Subjected to Vertical or Inclined Loads". *Journal of Geotechnical and Geoenvironmental Engineering, Vol. 140, No. 4.*

4. A. Ahmad (2012). "Simplified and Advanced Approaches for the Probabilistic Analysis of Shallow Foundations." PhD. Thesis, University of Nantes, France.

5. R.R. Barton (1992). "Metamodels for Simulation Input-Output Relations." Proceedings of the 1992 Winter Simulation Conference. Swain, J. J., et al. (eds.), Arlington, VA: 289-299.

6. G. Blatman, (2009). "Adaptive sparse polynomial chaos expansions for uncertainty propagation and sensitivity analysis." Ph.D thesis, Université Blaise Pascal, Clermont-Ferrand.

7. S.E. Cho, and H.C. Park (2010). "Effect of spatial variability of cross-correlated soil properties on bearing capacity of strip footing." International Journal for Numerical and Analytical Methods in Geomechanics, 34: 1-26.

Appendix A

One-dimensional Hermite polynomials

The one-dimensional Hermite polynomials are given by:

$$H_0(\xi) = 1$$
$$H_1(\xi) = \xi$$
$$H_2(\xi) = \xi^2 - 1$$
$$H_3(\xi) = \xi^3 - 3\xi$$
$$H_4(\xi) = \xi^4 - 6\xi^2 + 3$$
$$H_5(\xi) = \xi^5 - 10\xi^3 + 15\xi$$
$$H_6(\xi) = \xi^6 - 14\xi^4 + 45\xi^2 - 15$$
.
.
.
$$H_n(\xi) = \xi H_{n-2}(\xi) - H'_{n-1}(\xi)$$

Illustrative Example

In order to illustrate the PCE theory in a simple manner, a PCE of order p=3 using only M=2 random variables (ξ_1 and ξ_2) will be considered in this illustrative example. As may be easily seen from Table E.1, the PCE basis contains P=10 terms whose expressions $\Psi_\beta(\beta = 0,...,9)$ are computed using Equation (I.9).

β	Order of the term Ψ_β	$\Psi_\beta = \prod_{i=1}^{M} H_{\alpha_i}(\xi_i)$	$E\left(\Psi_\beta^2\right) = \prod_{i=1}^{M} \alpha_i !$
0	p=0	$\Psi_0 = H_0(\xi_1) x H_0(\xi_2) = 1$	$\alpha_1! \times \alpha_2! = 0! \times 0! = 1$
1	p=1	$\Psi_1 = H_1(\xi_1) x H_0(\xi_2) = \xi_1$	$\alpha_1! \times \alpha_2! = 1! \times 0! = 1$
2		$\Psi_2 = H_0(\xi_1) x H_1(\xi_2) = \xi_2$	$\alpha_1! \times \alpha_2! = 0! \times 1! = 1$
3	p=2	$\Psi_3 = H_1(\xi_1) x H_1(\xi_2) = \xi_1 \xi_2$	$\alpha_1! \times \alpha_2! = 1! \times 1! = 1$
4		$\Psi_4 = H_2(\xi_1) x H_0(\xi_2) = \xi_1^2 - 1$	$\alpha_1! \times \alpha_2! = 2! \times 0! = 2$
5		$\Psi_5 = H_0(\xi_1) x H_2(\xi_2) = \xi_2^2 - 1$	$\alpha_1! \times \alpha_2! = 0! \times 2! = 2$
6	p=3	$\Psi_6 = H_2(\xi_1) x H_1(\xi_2) = \left(\xi_1^2 - 1\right)\xi_2$	$\alpha_1! \times \alpha_2! = 2! \times 1! = 2$
7		$\Psi_7 = H_1(\xi_1) x H_2(\xi_2) = \xi_1\left(\xi_2^2 - 1\right)$	$\alpha_1! \times \alpha_2! = 1! \times 2! = 2$
8		$\Psi_8 = H_3(\xi_1) x H_0(\xi_2) = \xi_1^3 - 3\xi_1$	$\alpha_1! \times \alpha_2! = 3! \times 0! = 6$
9		$\Psi_9 = H_0(\xi_1) x H_3(\xi_2) = \xi_2^3 - 3\xi_2$	$\alpha_1! \times \alpha_2! = 0! \times 3! = 6$

Table A.1. Basis Ψ_β (β=0, …, 9) of the PCE and values of $E\left(\Psi_\beta^2\right)$ for a PCE with M=2 and p=3

By using Table A.1, one can write the PCE as function of the input random variables (ξ_1 and ξ_2) as follows:

$$\Gamma_{PCE}(\xi) = a_0\Psi_0 + a_1\Psi_1 + ... + a_9\Psi_9 = a_0 + a_1\xi_1 + a_2\xi_2 + a_3\xi_1\xi_2 + a_4(\xi_1^2 - 1) + a_5(\xi_2^2 - 1) + a_6\left(\xi_1^2 - 1\right)\xi_2 + a_7\xi_1\left(\xi_2^2 - 1\right) + a_8(\xi_1^3 - 3\xi_1) + a_9(\xi_2^3 - 3\xi_2) \quad \text{(A.1)}$$

Where the unknown coefficients can be computed using Equation (I.12). Once the PCE coefficients are computed, the first order Sobol indices for the two random variables (ξ_1 and ξ_2) can be easily obtained using the following equation $S(\xi_i) = \dfrac{\sum_{\beta \in I_i} \left(a_\beta\right)^2 E\left[\left(\Psi_\beta\right)^2\right]}{D_{PCE}}$.

The only additional step is to compute $E\left(\Psi_\beta^2\right)$ corresponding to these two random variables. Table A.1 provides the values of $E\left(\Psi_\beta^2\right)$ computed using the equation $E\left(\Psi_\beta^2\right) = \prod_{i=1}^{M} \alpha_i !$ for the different Ψ_β terms. The expressions of the first order Sobol indices of the two random variables ξ_1 and ξ_2 can thus be written as follows:

$$S(\xi_1) = \frac{a_1^2 + 2a_4^2 + 6a_8^2}{a_1^2 + 2a_4^2 + 6a_8^2 + a_2^2 + 2a_5^2 + 6a_9^2}; \qquad S(\xi_2) = \frac{a_2^2 + 2a_5^2 + 6a_9^2}{a_1^2 + 2a_4^2 + 6a_8^2 + a_2^2 + 2a_5^2 + 6a_9^2} \quad \text{(A.2)}$$

Where $I_1 = (1,4,8)$ and $I_2 = (2,5,9)$.